Reservoir Heterogeneity Effect on CO2 Storage

Investigate the effect of carbonate-cemented layers in the Roda Sandstone on the migration of the CO2 plume at a short-term timescale using RRM and DARTS

Majed Humoud Alghamdi

TU Delft

Reservoir Heterogeneity Effect on CO2 Storage

Investigate the effect of carbonate-cemented layers in the Roda Sandstone on the migration of the CO2 plume at a short-term timescale using RRM and DARTS

Thesis report

by

Majed Humoud Alghamdi

to obtain the degree of Master of Science
at the Delft University of Technology
to be defended publicly on September 4, 2023

Thesis committee:

Chair:	Prof. Dr. Allard W. Martinius
Supervisors:	Prof. Dr. Sebastian Geiger
	Dr. Denis Voskov
Student number:	5359716

An electronic version of this thesis is available at http://repository.tudelft.nl/.

Faculty of Civil Engineering and Geosciences · Delft University of Technology

Abstract

The storage of carbon dioxide is now regarded as a critical industrial application aimed at mitigating its accumulation in the atmosphere. Reservoirs and aquifers have been identified as viable alternative locations. This report seeks to examine the impact of sedimentological heterogeneity on the development and migration of CO2 plumes over time. The study uses the Roda Sandstone Formation as a case study, primarily due to the presence of carbonate-cemented layers within the Gilbert-delta lobes, which contribute to reservoir heterogeneity commonly observed in subsurface formations. The utilization of a sketch-based modeling approach was employed in constructing the geo-models represented by Rapid Reservoir Modeling (RRM) software since the Roda Sandstone is an exposed section in Isabena Valley in Spain. Furthermore, various realizations are constructed using different parameters of the cemented layers to comprehensively comprehend all potential scenarios. The aforementioned observations pertain to variations in the thickness and lateral continuity of the cemented layers. Additionally, dynamic modeling is also performed by injecting CO2 into the reservoir for 50 years. The simulator utilized for dynamic modeling is the Delft Advanced Research Terra Simulator (DARTS). The findings demonstrate that reservoirs with moderate sedimentological heterogeneity are actually better sites to store CO2 due to the capacity and effectiveness of the storage.

Acknowledgement

First, all praise is to Allah, Lord of the world, for all the successes and his blessing.

I would like to express my sincere gratitude to all individuals who played a significant role in obtaining my Master's degree from Delft University of Technology. I would like to acknowledge my family and friends for their patience and encouragement during this challenging period of my academic journey.

I am deeply thankful to my thesis supervisor, Prof. Dr. Allard W. Martinius, for his invaluable guidance, insightful feedback, and solid support throughout the research period. His expertise has been influential in shaping the path of this thesis study. I extend my profound thanks to the members of my thesis committee, Prof. Dr. Sebastian Geiger and Dr. Denis Voskov, for their thoughtful feedback and constructive suggestions that highly enriched the quality of my work.

I would like to express my gratitude to Saudi Aramco for sponsoring my master's degree.

Most importantly, I am indebted to my parents for everything in this life. I deeply thank my wife for her endless support and patience during my study. Special thanks to my son, Saad, as I saw you grow and started walking and talking during my master's study; they were gorgeous days. I am also thankful to my sisters and brothers for their nonstop support.

In closing, I am sincerely appreciative of the combined assistance and motivation that have accompanied me throughout this endeavor. The completion of this thesis owes its existence to the invaluable support from each individual and institution acknowledged earlier.

Thank you.

Majed Humoud Alghamdi
September 4th, 2023

Contents

Nomenclature

List of Abbreviations

BHP	Bottomhole pressure
EOR	Enhanced Oil Recovery
FA	Facies Association
GR	Grid Resolution
HST	Highstand System Tract
INJ	Injector
itor	iterator
LST	Lowstand System Tract
mD	Millidarcy
MFS	Maximum flooding surface
NE	Northeast
NW	Northwest
RA	Remove Above
RAI	Remove Above Intersection
RB	Remove Below
RBI	Remove Below Intersection
RQ	Research Question
RRM	Rapid Reservoir Modeling
SB	Sequence boundary
SE	Southeast
Sgr	Residual saturation
SM	Shelf-margin
SR	Select Region
SW	Southwest
Swc	Connate water saturation
TRT	Transgressive System Tract

List of Figures

List of Tables

1

Introduction

The atmospheric concentration of Carbon dioxide (CO2) has reached a significantly elevated state, and it negatively impacts the environment. In order to effectively mitigate the anthropogenic role in this concentration, it is imperative to find alternative giant locations that are capable of accommodating this gas. Studies suggest that significant quantities are present in the subsurface, specifically in porous reservoirs and aquifers, and can be used for CO2 sequestration. Indeed, the practice of injecting CO2 into oil reservoirs for the purpose of optimizing oil recovery, commonly referred to as "enhanced oil recovery - EOR," has been implemented for several decades. Thus, the technology has attained a well-established status. Research in this area should derive advantages from the tools and methods created for uncertainty analysis of oil and gas reservoirs.

In this thesis study, Roda Sandstone Formation will be studied and examined for subsurface storage of CO2 studies. Roda Sandstone is an outcrop that is exposed in Isabena Valley in Spain. Geologically, Roda Sandstone Formation is made of a complex environment and is considered an excellent example of reservoir heterogeneities. Geological heterogeneities exist in most subsurface reservoirs and aquifers; therefore, it would be good to investigate how the CO2 behaves when injected into such a reservoir or aquifer.

Scientific studies show that the CO2 is primarily trapped at a short-term timescale (<100 years) by structural and stratigraphic trapping and then residual trapping. While at medium-term and long-term (>10,000 years) timescales, solubility and mineral trapping tend to be increased (Gibson-Poole et al., 2009[1]; Ajayi et al., 2019[2]). These trapping mechanisms are shown in Figure 1.1 with respect to injection time and contribution.

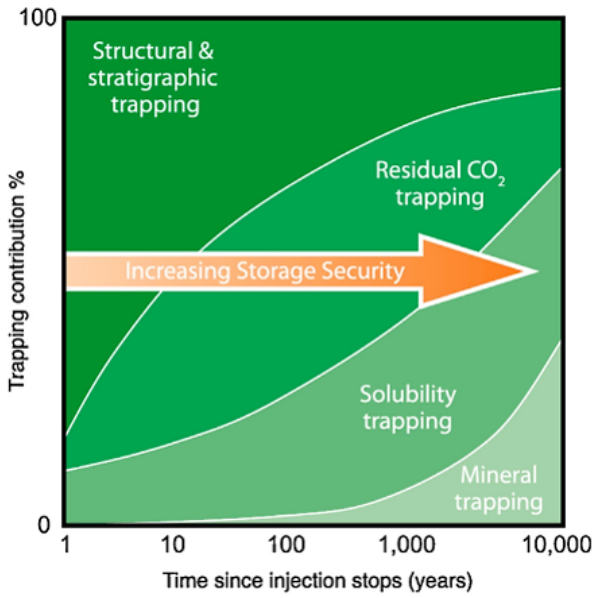

Figure 1.1: Various trapping mechanisms for CO_2 over time [3]

1.1. Research Question & objective

The aforementioned points led to questions that formed the purpose of this thesis study:

Research Questions

Does the presence of impermeable layers in the reservoir have an influence on the CO2 plume?
How would the CO2 plume move if carbonate-cemented strata were present?
Which kind of reservoir, homogeneous or heterogeneous, is preferable for CO2 storage?

Research Objective

The primary objective of this thesis study is to examine and analyze the role of reservoir heterogeneity, particularly the Roda carbonate-cemented layers, on the movement and evolution of a CO2 plume over a period of 50 years (short-term timescale).

1.2. Structure of the Report

The structure of this thesis project leads the division into two distinct sections. The first section of this study provides a comprehensive overview of the research's geological settings, covering the structural geology of the designated study area, along with a description of the sedimentology and sequence stratigraphy of the Roda Sandstone formation, highlighting its characteristic sedimentological heterogeneity. The main part of this study is the second section, which can be seen in Figure 1.2. It covers the project's key datasets and demonstrates how to construct a geo-model using Rapid Reservoir Modeling (RRM) and the dynamic simulator known as Delft Advanced Research Terra Simulator (DARTS). Then, it shows the created geo-models with their petrophysical properties. After that, it dives into the dynamic simulation for all the geo-models. In the end, the study's findings will be thoroughly analyzed and interpreted in the discussion chapter, leading to a comprehensive conclusion regarding the investigation of the research.

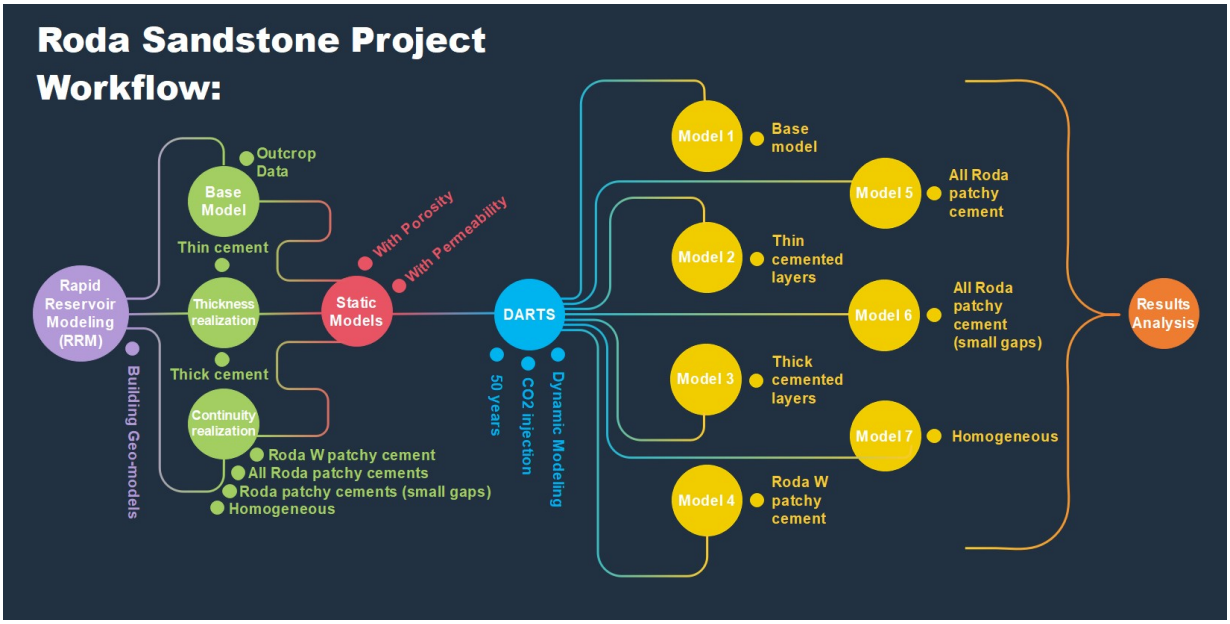

Figure 1.2: The structure of the project from Modeling to Discussion

2

Geological Setting

This chapter will describe the structural processes that underwent in the study region in the Pyrenees, as well as the sedimentology and sequence stratigraphy of the Roda Sandstone, in order to provide a foundation for understanding the geology of the reservoir.

2.1. Structural Settings

From the Late Cretaceous to the Later Miocene, the convergence of the Iberian and Eurasian plates led to the formation of the Pyrenees, an East-West trending Alpine orogen (Puigdefàbregas & Souquet, 1986 [4]; Dewey et al., 1989 [5]; Srivastava et al., 1990 [6]; Roest & Srivastava, 1991 [7]; Olivet, 1996) [8]. The uplift of the Pyrenees caused the inversion of faults throughout the Mesozoic extensional rift basin. The Aquitanian Basin formed in the north, and the South Pyrenean Foreland Basin formed in the south. The Boixols, Cotiella-Montsec, and Serres Marginal Thrust Sheets form a north-to-south oriented, imbricated cover thrust system in the southern Pyrenees (Fig 2.1). These thrust sheets evolved as a piggy-back thrusting sequence throughout the Late Cretaceous, Palaeocene-Early Eocene, and Middle Eocene-Oligocene eras, respectively (Garrido-Megias & Rios, 1972 [9]; Munoz, 1992 [10], 2002 [11]; Meigs, 1997 [12]). At the present time, these thrust sheets are located on top of the Tertiary sediments that constitute the Ebro Foreland Basin (Fig 2.2).

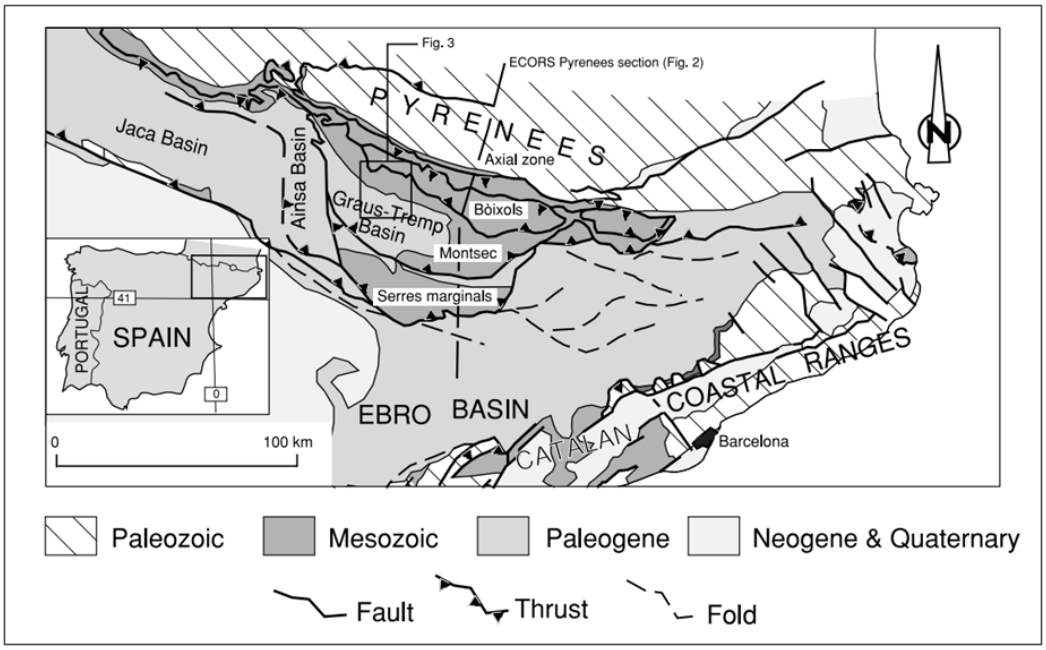

Figure 2.1: Geological map shows the structural elements at the studied area (López et al.,2003)

The initial synorogenic deposits of the South-Pyrenean Foreland Basin are composed of late Santonian and Campanian turbidites. These sediments were formed during the inverse of Early Cretaceous extensional faults known as the Boixols Thrust (Bond & McClay, 1995; McClay et al., 2002)[13][14]. The Upper Cretaceous sediments were deposited in the area that was examined concurrently with the development of the folds, namely Turbón and Serrado anticlines, along the Boixols Thrust side (Figs 2.1 and 2.2).

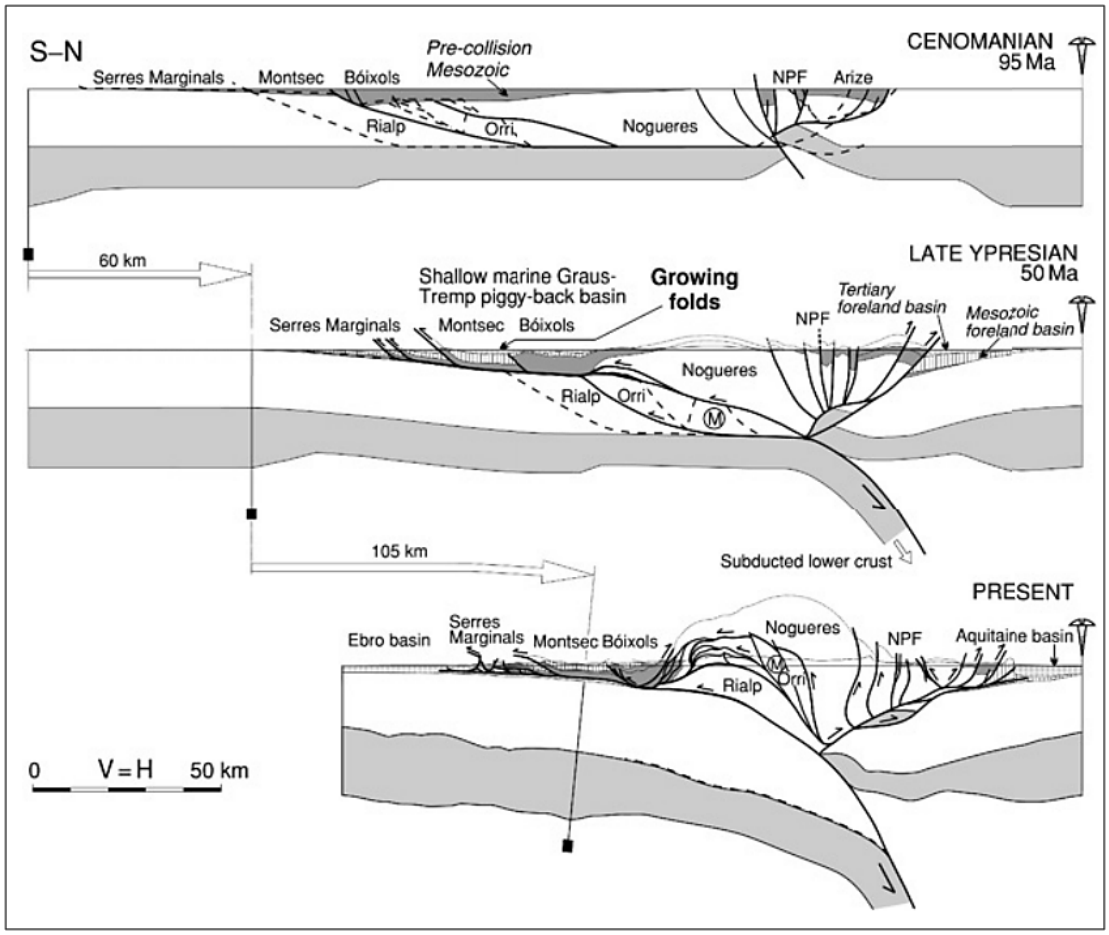

Figure 2.2: Structural profile of the area before the convergence (upper), Early Eocene (middle), and at present (lower) (López et al.,2003)

Throughout the Paleocene and Early Eocene time periods, thrust propagation into the Montsec foreland created a new phase of the South-Pyrenean Foreland Basin. Hence, the Graus-Tremp Basin formed as a piggyback basin over the Montsec Thrust Sheet.

Subtle folds formed during underlying thrust displacement, altering the morphology of the shallow marine depositional environment of the Roda Sst Mbr in the Isábena valley (Eichenseer, 1988 [15]; López-Blanco, 1996 [16]; López-Blanco et al., 2003). Benthic foraminiferal occurrence patterns in transgressive facies assemblages; variations in sandstone paleocurrent due to the existence of sedimentary trough features formed by the growth of a syncline; thicker sedimentary units above synclines and thinner over anticlinal structures; development of carbonate platform on top of anticlinal structures. Seismic data have provided evidence of synsedimentary folding (López-Blanco, 1996; López-Blanco et al., 2003).

2.2. Sedimentology and stratigraphy Settings

2.2.1. Roda formation and stratigraphy

The area of interest was located at the margin of the Tremp-Graus Basin during the Eocene, particularly on the northeastern side (Fig. 2.1), and the first establishment of the sedimentary infill of the Isabena Valley was done by Mey et al. (1968)[17] and Schaub (1973)[18], and then modified by Nijman and Nio (1975)[19]. According to Nijman and Nio (1975), the infill of the Tremp-Graus Basin began with the Ager Group. This Ager group is characterized by having marginal and shallow facies in the east and shifts into open marine facies towards the west. Stratigraphically, the Ager group consists of 5 formations and they are bounded by unconformity at the Late Palaeocene to Early Eocene. These formations include Serraduy, Puebla Limestone, Roda, Morillo and San Esteban formations (Fig. 2.3)(Nijman and Nio, 1975). Focusing on Roda Formation, its deposits are characterized by approximately 200 m thick of a shallow-marine, mixed siliciclastic–carbonate succession (Martinius and Molenaar, 1991). Based on the biostratigraphic data, it belongs to the late Ypresian in age (Samso et al., 1990; Tosquella et al., 1990)[20]. The Ypresian Roda Formation is overlain and underlain by the Puebla Limestone Formation and Morillo Limestone Formation, respectively. Additionally, Plateau Limestone is deposited between members of the Roda Formation, which represents stable conditions of the basin as shown in Figure 2.3 (Molenaar et al., 1988[21]; Nio and Yang, 1990[22], 1991b[23]; Michaud & Dalrymple, 2016[24]).

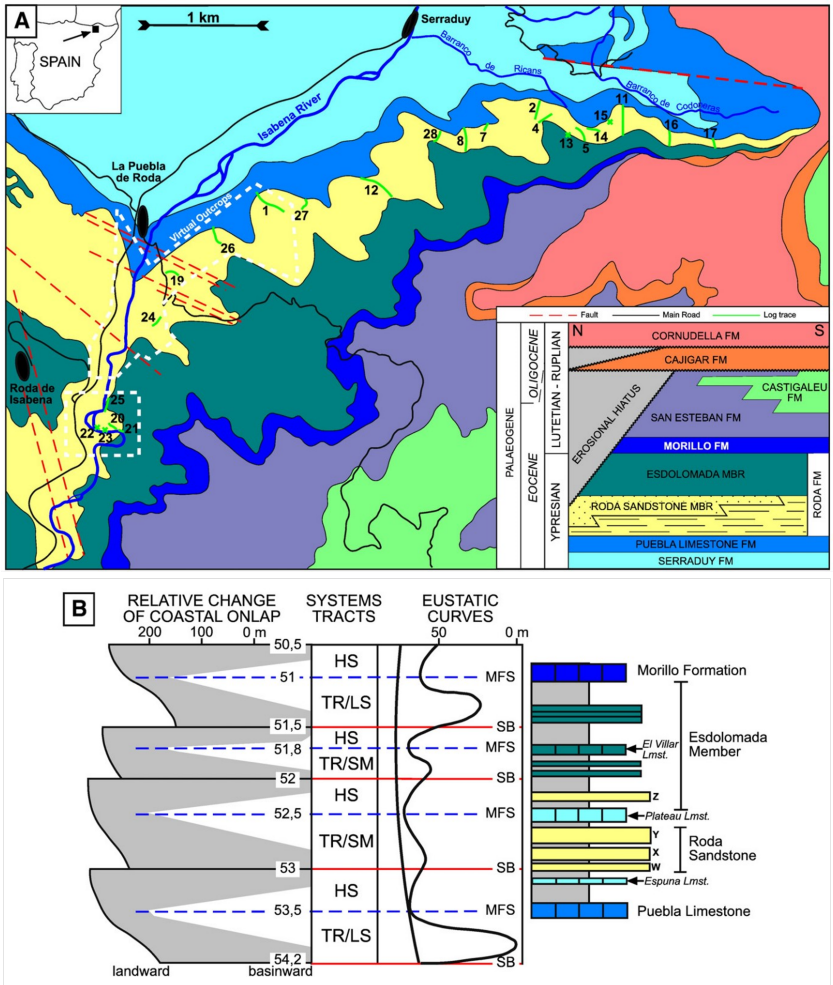

Figure 2.3: (A) Geological map of the northern Isabena Valley showing measured log sections (explained in the next section) and the lithostratigraphic column, modified from Molenaar (1990). (B) Stratigraphic section ranging from Puebla to Morillo formations exhibiting sequences and system tracts (Nio & Yang, 1991b). Abbreviations MFS: maximum flooding surface, SB: sequence boundary, SM: shelf-margin, HS: highstand, TR: transgressive, and LS: lowstand (Leren et al., 2010)

For the stacking pattern of the Roda Formation, it starts with an overall progradation towards S and SW which represents the Roda Sandstone Member, followed by retrogradation and aggradation as the lower and the upper parts of the Esdolomada Member, respectively (Fig. 2.3B) (Tosquella, 1988[25]; Crumeyrolle et al., 1992[26]; Lopez-Blanco, 1996; Lopez-Blanco et al., 2003[27]; Leren et al., 2010).

The Roda Formation is divided into six main Gilbert-type delta lobes; ranging from Roda U to Z (Lopez-Blanco, 1996). The first five Roda lobes (U to Y) are composed of sandstone bodies that are covered by thin submarine hardgrounds, which are characterized by heavily bioturbated and fossiliferous calcareous sandy beds. These five Roda lobes belong to Roda Member, while Roda Z lies within the Esdolomada Member (Fig. 2.3B)(Molenaar et al., 1988; Martinius and Molenaar, 1991).

The sand bodies comprising the Gilbert-type delta lobes consist of multiple sub-lobes at a smaller scale (Nio and Siegenthaler, 1978[28]; Puigdefabregas et al., 1987[29]; Yang and Nio, 1989[30]; Crumeyrolle et al., 1992; Lopez-Blanco, 1996; Molenaar and Martinius, 1996[31]; Crumeyrolle, 2003[32]; Lopez-Blanco et al., 2003; Tinterri, 2007[33]; Leren et al., 2010). In general, these smaller-scale sub-lobes are stacked (laterally and vertically), and although they follow the main sediment input direction of the Gilbert-type delta, there is noticeable switching of these inner-lobes as shown in Figure 2.4. They consist of large-scale foresets that can reach heights of up to 15 meters. These foresets dip towards the basin at an angle of up to 32 degrees. For the topsets, normal regression in addition to differential subsidence allows the preservation of the delta sub-lobes topsets in medial and distal environments (Lopez-Blanco, 1996; Martinius, 2017).

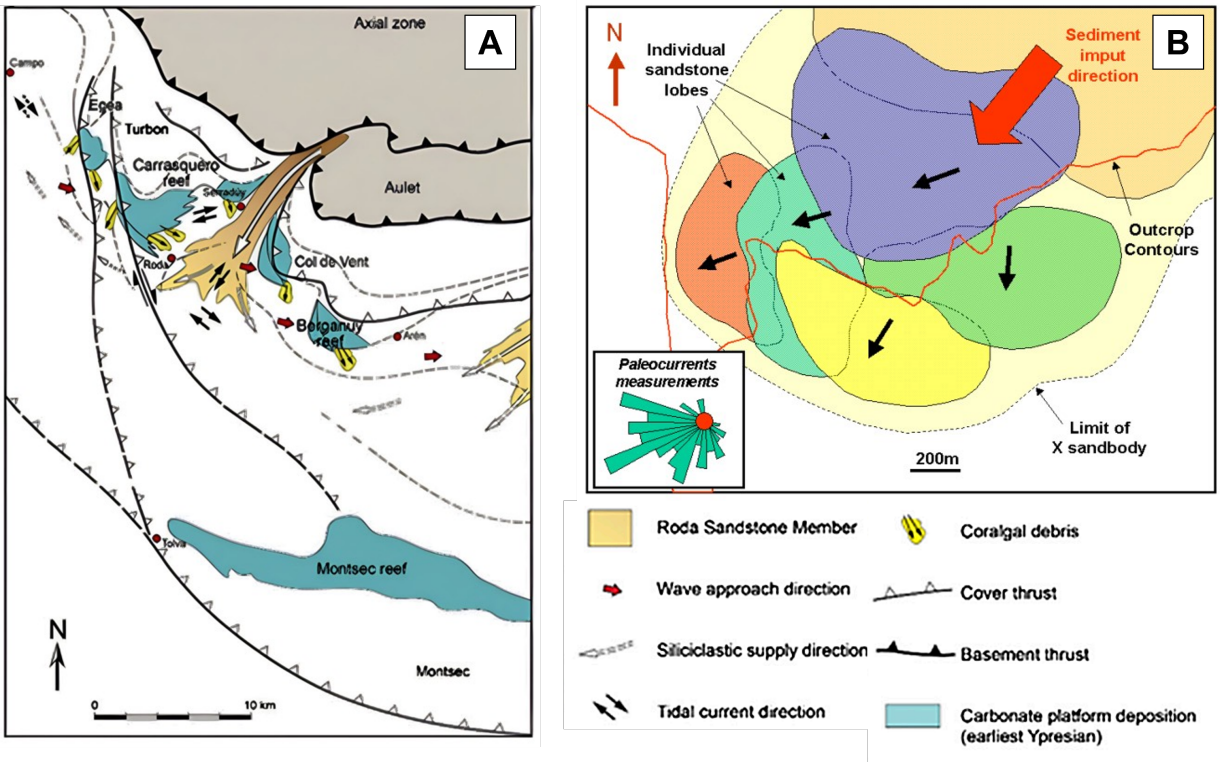

Figure 2.4: (A) The direction of the sediment input (Martinius, 2017 After Eichenseer, 1988). (B) Roda Sandstone sub-lobes switching in direction (Crumeyrolle, 2003)

2.2.2. Depositional environment: Facies and facies associations

The Isabena Valley has been the site of several 1D logs. Details like lithologies, structures, and textures have been recorded in these logs by the previous work (Leren et al., 2010). And as can be seen by the representative logs in Figure 2.5, different types of facies have been observed in the Roda Sandstone Member. Additionally, the facies vary from conglomerate and coarse sandstone to finer and muddier facies as moving from N – NE towards S-SW, reflecting proximal to distal depositional settings (Dubrule et al., 1994[34]; Crumeyrolle, 2003).

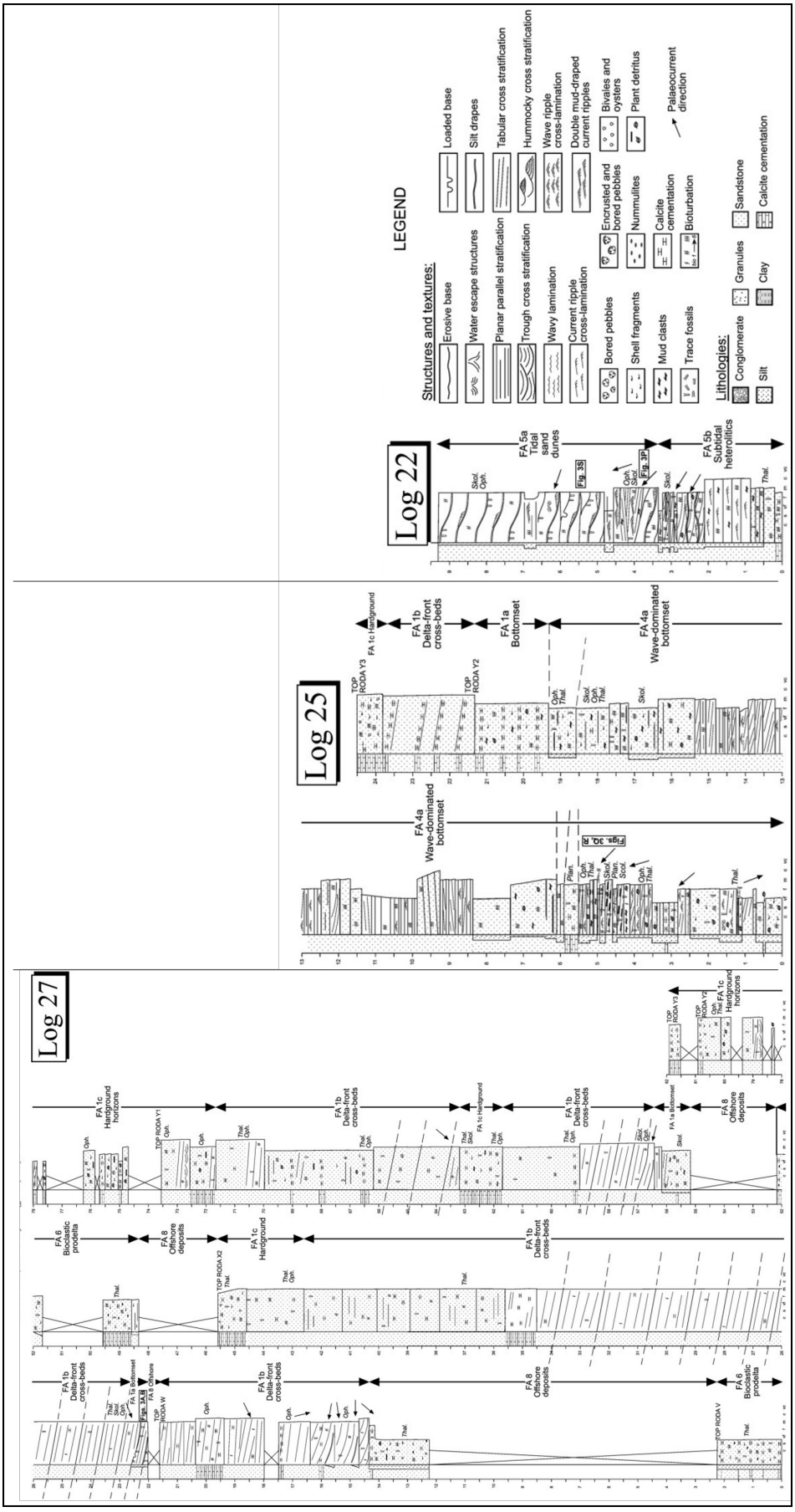

Figure 2.5: Three logged sections from Roda Sandstone Formation at the Isabena Valley have. Log 27 shows Roda W, X, and Y with their facies associations. It has been used as the reference for the thickness of the carbonate-cemented layers at the center of these lobes as the section is located. Log 25 and 22 demonstrate the distal part of Roda Y as they are logged in further into SW as the progradation of the lobes occurred. And they are an example of the modified delta deposits (Leren et al., 2010).

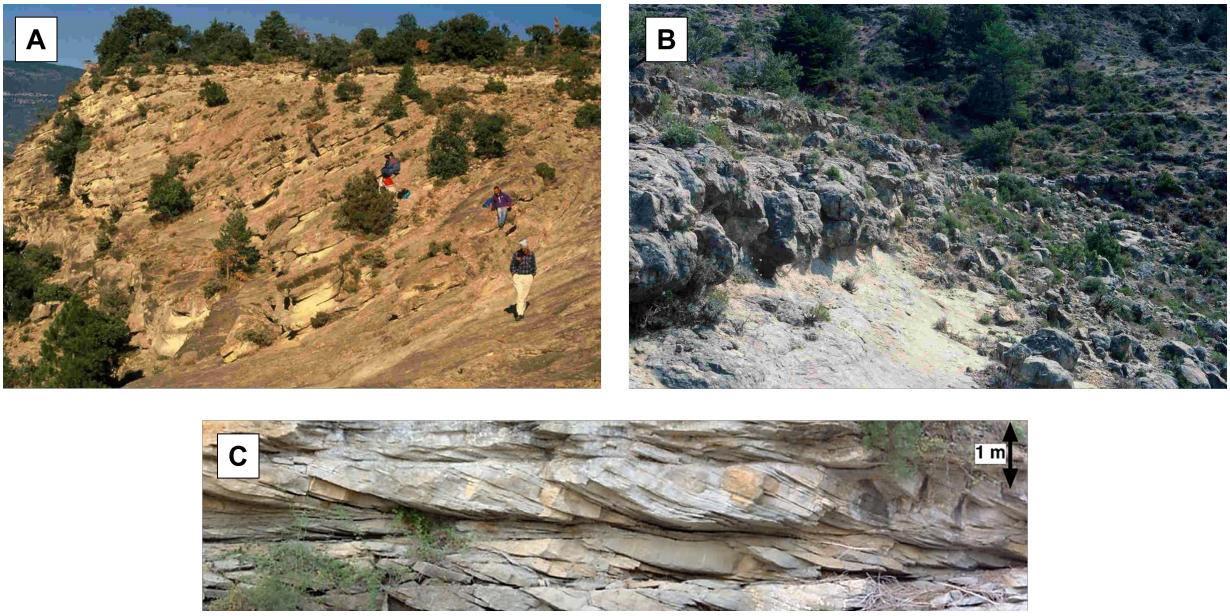

Figure 2.6: (A) an outcrop photograph showing sets of clinoforms of a sand lobe composed of medium to coarse sands (Crumeyrolle, 2003). (B) carbonate-cemented bed capping one of the prograding sand lobes (Crumeyrolle, 2003). (C) photograph of a tidal bundle cycle with a dune in the center (Martinius, 2017)

According to Leren et al. (2010), eight facies associations have been recognized from the measured sections. These facies associations are summarized in the following:

- Delta-front deposits: medium to coarse sandstone, the dominant sandstone beds along the Isabena Valley that are deposited over all Roda W-Z lobes. Each set is nearly 25 m thick and laterally continuous along the dip direction (up to 5 km). Furtherly, it has been divided into three sub-facies. These sub-facies associations include massive bottomset, large-scale cross-bedded and hardground bioclastic sandstones (Orton & Reading, 1993)[35]. Figure 2.6 shows the delta-front deposits outcrop.
- Medial shoal-water fan-delta deposits: massive coarse-grained sandstone (with few cross-stratification and ripples), 1–15 m thick vertically and up to one km laterally along the strike along Barranco de Codoñeras (Postma & Drinia, 1993)[36].
- Shoreface deposits: locally, less than 1 km along the dip and strike, 5-40 m thick, massive medium to coarse sandstones with minor hummocky, tabular cross-stratification, and wave-ripples.
- Wave-modified delta deposits: 1-40 m thick of very fine to medium sandstone with wave ripples.
- Tidally-modified delta-front deposits: Alteration of sandstones and mud drapes, composed of tidal dune sandstones and subtidal heterolithics, found in Roda Y along the Isabena Valley, mud drapes are up to 5 cm, subtidal dunes in Roda Y were created by regional ebb-tidal currents flowing towards the northwest (Dalrymple, 1992, 2010)[37][38] (Figure 2.6C and 2.7).
- Bioclastic prodelta: composed of massive, bioclastic, very fine-grained sandstones to siltstones, Thickness up to 5 m, continuous along dip, the dominant bioclastic indicates quite stable conditions.
- Interlobe deposits: restricted and poorly exposed, muddy siltstones (less than 5 m thick), abundant plant debris, considered as sub-environments on a shoal-water fan delta.
- Offshore deposits: composed of greyish muddy siltstones that are laterally continuous along the dip, deposited below SWWB (storm weather wave base) with dominantly hemipelagic deposits.

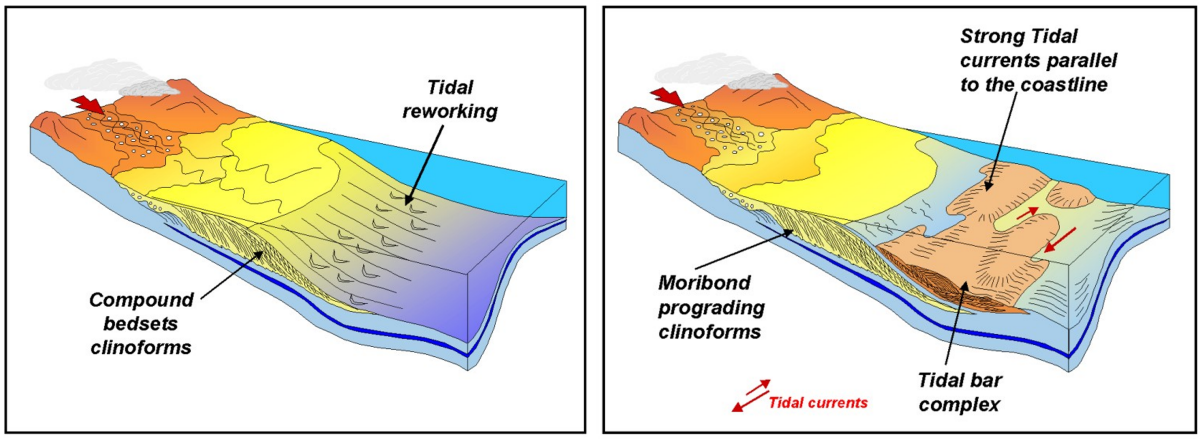

Figure 2.7: A schematic model illustrating the evolution of tidal bars in the Roda Y lobe and their relationship to the position and orientation of prograding clinoforms.(Crumeyrolle, 2003)

By compiling the 1D logs data, Leren et al. (2010) and Martinius (2017) have constructed a cross-section based on the logs correlations with their comprehension of the facies associations observed in the Roda sandstone outcrops. The depicted cross-section illustrates the eastern side of the Isabena Valley, oriented in a northeast to southwest direction, which aligns with the Roda Gilbert-type delta lobes progradation direction. Figure 2.9 shows this cross-section.

Figure 2.8: photograph of the eastern side of the Isabena Valley showing Roda Sandstone outcrop

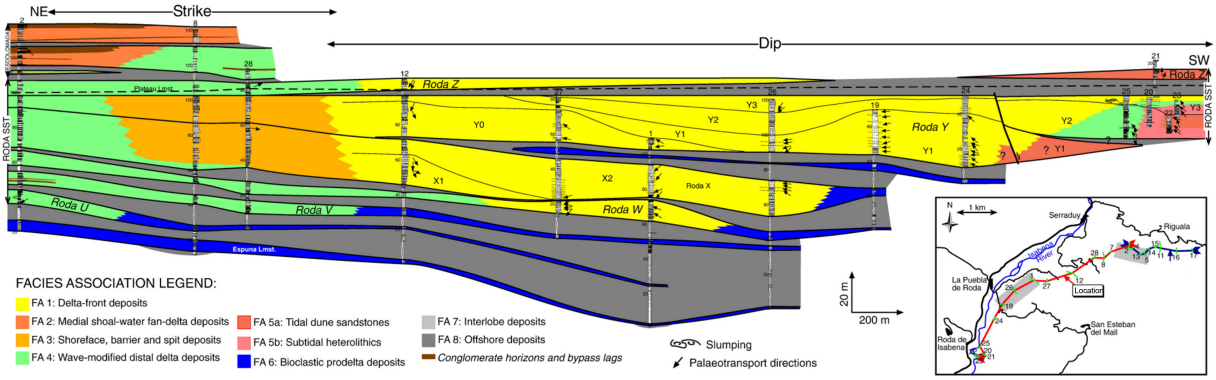

Figure 2.9: NE-SW x-section was made by correlating the recorded logs from the Roda outcrops along the eastern side of the Isabena Valley (Leren et al., 2010)

2.2.3. Carbonate cementation and development

The subsequent section of this report will be dedicated to an elaborate discussion of the carbonate-cemented layer, owing to its paramount significance within the context of the report. The aforementioned layer constitutes an integral component of the delta-front deposits, more precisely identified as the hardground bioclastic sandstone. These layers are developed on top of the delta lobes and sub-lobes of Roda Formation (Coll et al., 2013)[39].

According to Gaemers (1978), the Tremp-Graus Basin was located near the tropical, swamps and coastal during the deposition of the Ypresian Roda Formation, which justifies the presence of coral reefs, large foraminifera (Jimenez, 1987), calcareous green algae (Gaemers, 1978) and wood fragments (Martinius, 1991) in Roda Formation in addition to the existence of a shallow carbonate platform in the south on the Montsec High, which is considered as a structural high (Molenaar & Martinius, 1996).

In the mixed system (siliciclastic-carbonate), the quantity of carbonate nuclei present and the length of time that no sediment supply occurs during the cementation development process determine the extent to which these layers are lithified (Martinius, 2017). As a result of lobe switching and faunal abundance, lithified carbonated-cemented strata have developed above Roda lobes and sub-lobes (Fig.2.6B)(Molenaar & Martinius, 1996). The development of carbonate cementation in the Roda Formation occurred in three distinct stages (Martinius & Molenaar, 1991)[40]. In the first phase, the accumulations of fringe cement formed around the siliciclastic grains of the delta-front deposits and appeared as nodules. These nodules are noticeably found in the mega-foresets of the Gilbert-delta lobes, which reflect the short time gaps between the sediment supplies of the Roda lobes. Then, when these individual nodules started amalgamating laterally, sandstones between these nodules became partially lithified. This stage is known as the intermediate stage of hardground development. Lastly, the third stage occurred when the cessation of sedimentation happened for a prolonged time, and the surface was extensively colonized by fauna. This phase's bioturbation and fringe cementation contributed to developing a fully lithified layer (Fig.2.10).

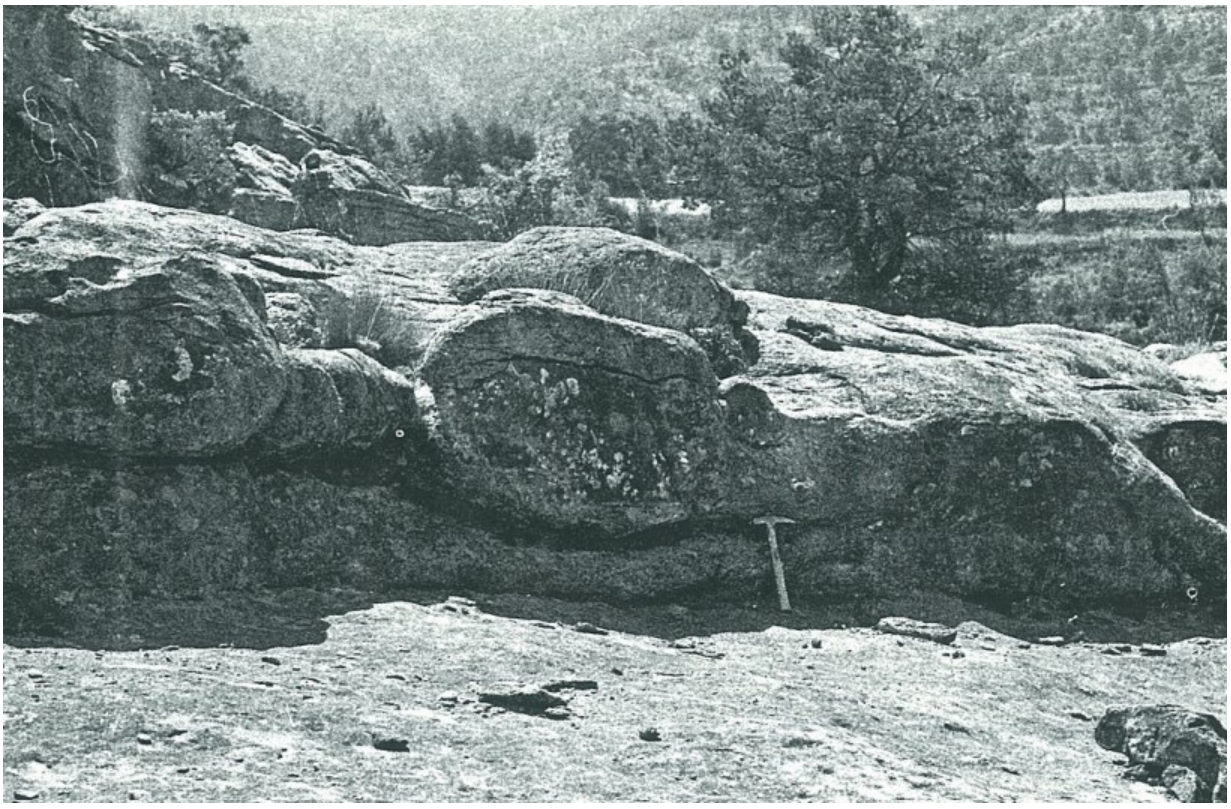

Figure 2.10: well-lithified layer of Roda sandstone with nodular structures (Molenaar & Martinius, 1990)[41]

Because of their different development stages, it is crucial to analyze how these carbonated-cemented units may affect CO2 subsurface storage when they exist in the reservoir.

3

Datasets

The datasets can be divided into two distinct parts. The First section comprises the geological outcrop data that were methodically obtained and skillfully gathered through fieldwork. And the second section of this chapter refers to the petrophysical data that will be assigned to the models for each facies. This chapter is structured in a manner that each part will be provided in an individual section.

3.1. Geological Data

To build an accurate model of the Roda Sandstone Formation, certain data is required. Therefore, geological data for Roda W, X, and Y are presented below. These data include parameters such as the number of layers, lobe thickness, lobe dimensions, and delta-front and carbonate-cemented characteristics. The characterization of the facies has been taken from the logged sections in the previous chapter (Figure 2.5). In this project, Roda W, X, and Y were adopted from the research of Leren et al. (2010) in terms of their overall shape and orientation. As shown in Figure 3.1, the delta-front deposits in all lobes are directed toward SW, while the tidally-modified delta-front deposits have an N-NW direction.

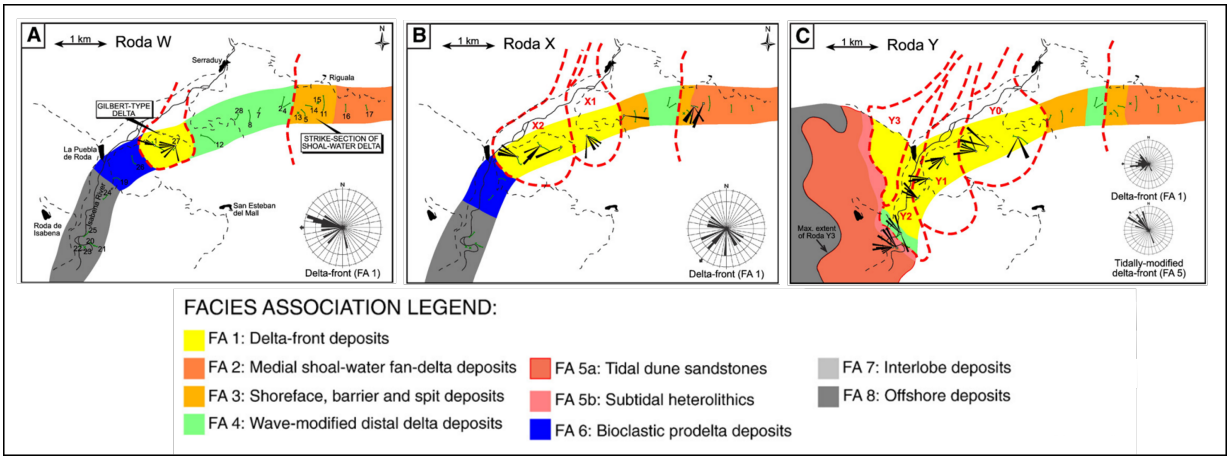

Figure 3.1: The dashed red lines in A, B, and C show the delta lobes' extensions. Map A is Roda W with a single Gilbert-type delta that directed SW. Map B is the extension and direction of Roda X, composed of two Gilbert-type sub-lobes (X1–X2). Map C is for Roda Y with its four Gilbert-type lobes that consist of delta-front deposits directed toward the southwest with north-westward tidally-modified delta-front deposits (Leren et al., 2010)[42].

The thickness of each lobe and its carbonate-cemented layer is taken from three logged sections, as shown in Figure 2.5. In addition, the dimensions of each lobe are approximated with their carbonate-cemented characteristics. Based on the shape and the thickness of all Roda Gilbert-type sub-lobes, Roda W is the smallest compared to Roda X and Y, while Roda Y is the most progradational lobe. Tables 3.1, 3.2, and 3.3 display these details for Roda W, X, and Y, respectively.

Table 3.1: Parameters and dimensions of the main Roda W lobe

Data of Roda W Lobe	
Number of sub-lobes	1
Sandstone Thickness	8 - 15 m
Length of Sand-lobe	2 Km
Width of Sand-lobe	0.4 - 1 Km
Carbonate-cemented Layer Thickness	0.9 m
Lateral continuity of carbonate-cemented Layer	fully developed

Table 3.2: Parameters and dimensions of the main Roda X lobe

Data of Roda X Lobe	
Number of sub-lobes	2
Sandstone Thickness	17 - 25 m
Length of Sand-lobe	2.7 Km
Width of Sand-lobe	0.5 - 1.3 Km
Carbonate-cemented Layer Thickness	1 m
Lateral continuity of carbonate-cemented Layer	fully developed

Table 3.3: Parameters and dimensions of the main Roda Y lobe

Data of Roda Y Lobe	
Number of sub-lobes	4
Sandstone Thickness	27 - 41 m
Length of Sand-lobe	3.6 Km
Width of Sand-lobe	0.6 - 2 Km
Carbonate-cemented Layer Thickness	1 m
Lateral continuity of carbonate-cemented Layer	fully developed

The modeling of the Roda Sandstone Formation will make use of all of the data that were obtained and interpreted from the outcrop. These data will be utilized as the input parameters of the base model. The other realizations will employ the same data, but they will vary from each other in terms of their three-dimensional presentations. These specifications will be discussed in the modeling section of each scenario.

3.2. Petrophysical Data

There is a lack of petrophysical data, especially permeability data, for the Roda Sandstone Formation. Subsurface data from a similar formation will be used to get overcome this obstacle. When choosing data for reservoir characteristics, it is most important to prioritize similarities in the depositional environment. As a result, the Sognefjord Formation from the Troll field is considered as the petrophysical input data for Roda Sandstone Modeling.

The Sognefjord Formation was reached at a depth of 1440 m by Well 31/2-1 in the Troll field (Figure 3.2). As can be seen in Figure 3.2, the reservoir has a porosity of 30% and a permeability of 1000 mD, both determined by the post-drilling analysis report. As an outcome, these values are going to be applied to the Roda sandstone intervals for the vertical and horizontal directions.

Well: 31/2-1

Top depth [m]	Lithostrat. unit
348	NORDLAND GP
525	HORDALAND GP
1184	ROGALAND GP
1184	BALDER FM
1250	SELE FM
1322	LISTA FM
1393	VÅLE FM
1405	CROMER KNOLL GP
1414	VIKING GP
1414	DRAUPNE FM
1440	SOGNEFJORD FM
1532	HEATHER FM
1595	FENSFJORD FM
1742	KROSSFJORD FM
1880	HEATHER FM

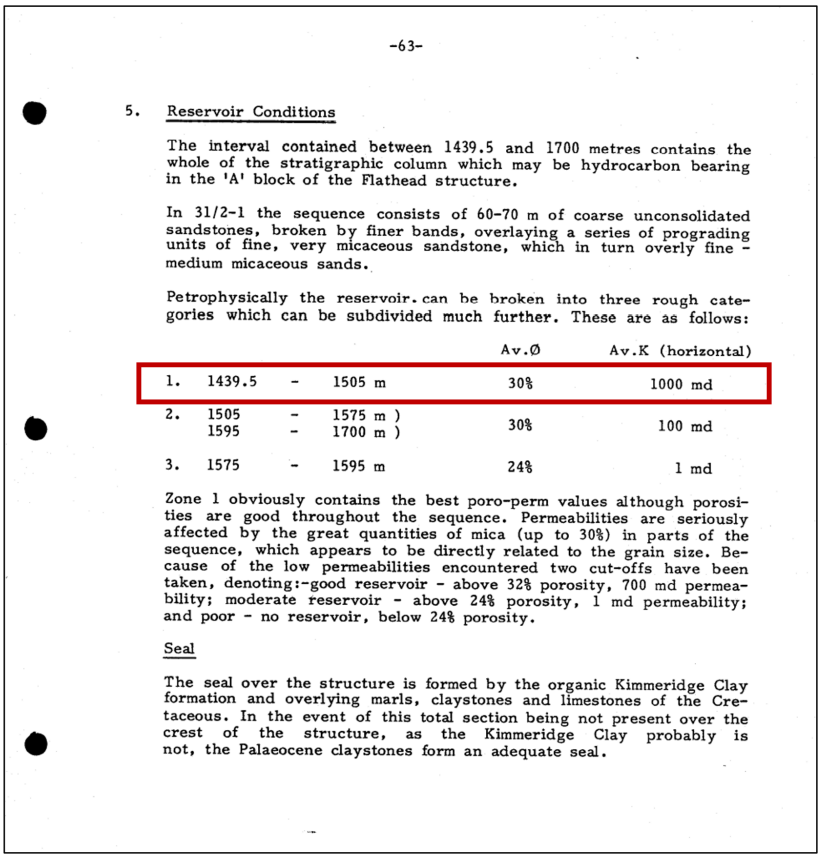

-63-

5. Reservoir Conditions

The interval contained between 1439.5 and 1700 metres contains the whole of the stratigraphic column which may be hydrocarbon bearing in the 'A' block of the Flathead structure.

In 31/2-1 the sequence consists of 60-70 m of coarse unconsolidated sandstones, broken by finer bands, overlaying a series of prograding units of fine, very micaceous sandstone, which in turn overly fine - medium micaceous sands.

Petrophysically the reservoir can be broken into three rough categories which can be subdivided much further. These are as follows:

			Av.Ø	Av.K (horizontal)
1.	1439.5 -	1505 m	30%	1000 md
2.	1505 -	1575 m)	30%	100 md
	1595 -	1700 m)		
3.	1575 -	1595 m	24%	1 md

Zone 1 obviously contains the best poro-perm values although porosities are good throughout the sequence. Permeabilities are seriously affected by the great quantities of mica (up to 30%) in parts of the sequence, which appears to be directly related to the grain size. Because of the low permeabilities encountered two cut-offs have been taken, denoting:-good reservoir - above 32% porosity, 700 md permeability; moderate reservoir - above 24% porosity, 1 md permeability; and poor - no reservoir, below 24% porosity.

Seal

The seal over the structure is formed by the organic Kimmeridge Clay formation and overlying marls, claystones and limestones of the Cretaceous. In the event of this total section being not present over the crest of the structure, as the Kimmeridge Clay probably is not, the Palaeocene claystones form an adequate seal.

Figure 3.2: Well: 31/2-1 showing Sognefjord Formation with its petrophysical properties, which is considered as an analogue for Roda Sandstone (NPD Factpage, 2023)[43].

Clarehugh (2018) analyzed the composition of the carbonate-cemented strata by analyzing thin sections and QEMSCAN images as can be observed in Figure 3.3. From these images, no visual porosity can be observed; thus, the layer is impermeable. So, the assumed values of the porosity and permeability are 0.1% and 0.001 mD, respectively.

For tidally-modified delta-front deposits, Martinius (2017) extensively studied and modeled this unit. Mud drapes are prevalent in this tidally-affected unit. These mud drapes and their cements play a significant role in permeability, mainly the vertical ones, they reduce the overall porosity and kv/kh. This unit's porosity and permeability will be averaged. By comparing the vertical with the horizontal values from these models, approximately a factor of 10 is between these two values. Thus, horizontal permeability will be 500 mD and vertical permeability 50 mD. Figure 3.4 shows the models of this unit by Martinius (2017).

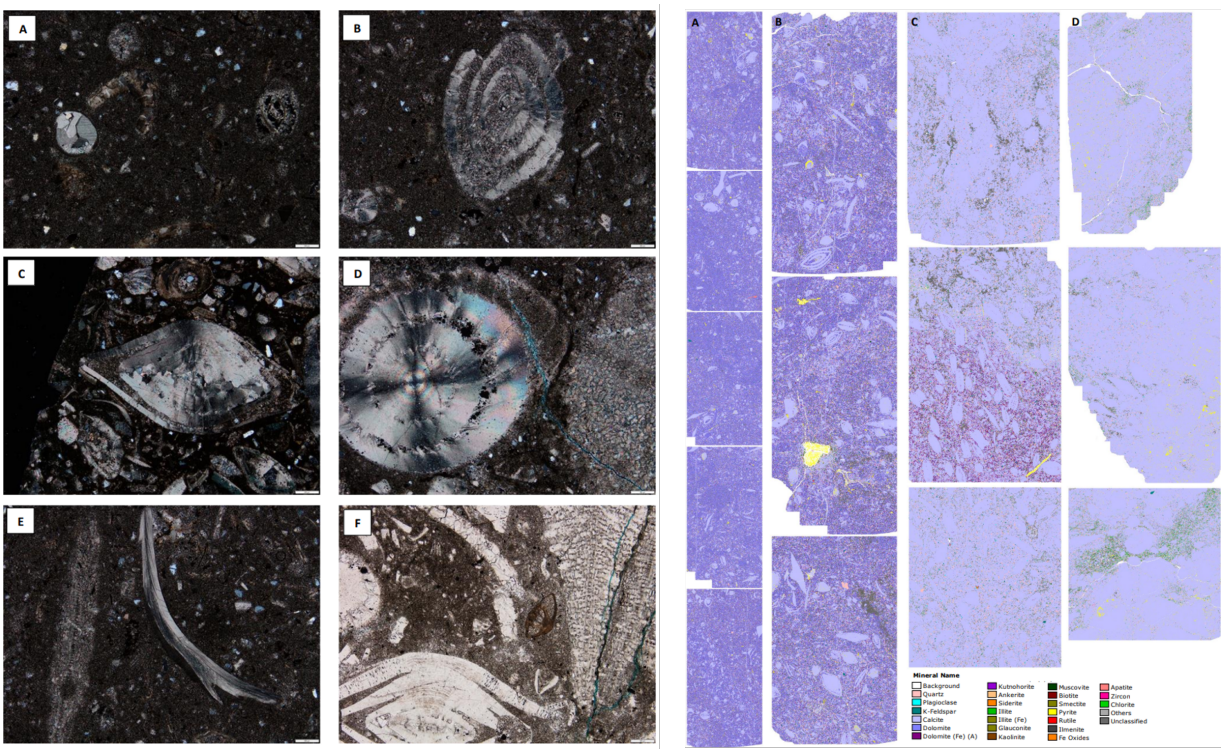

Figure 3.3: Thin sections and images to display the bioclastic and mineralogy of the carbonate-cemented layers. No visual porosity can be observed. (Clarehugh, 2018)[44].

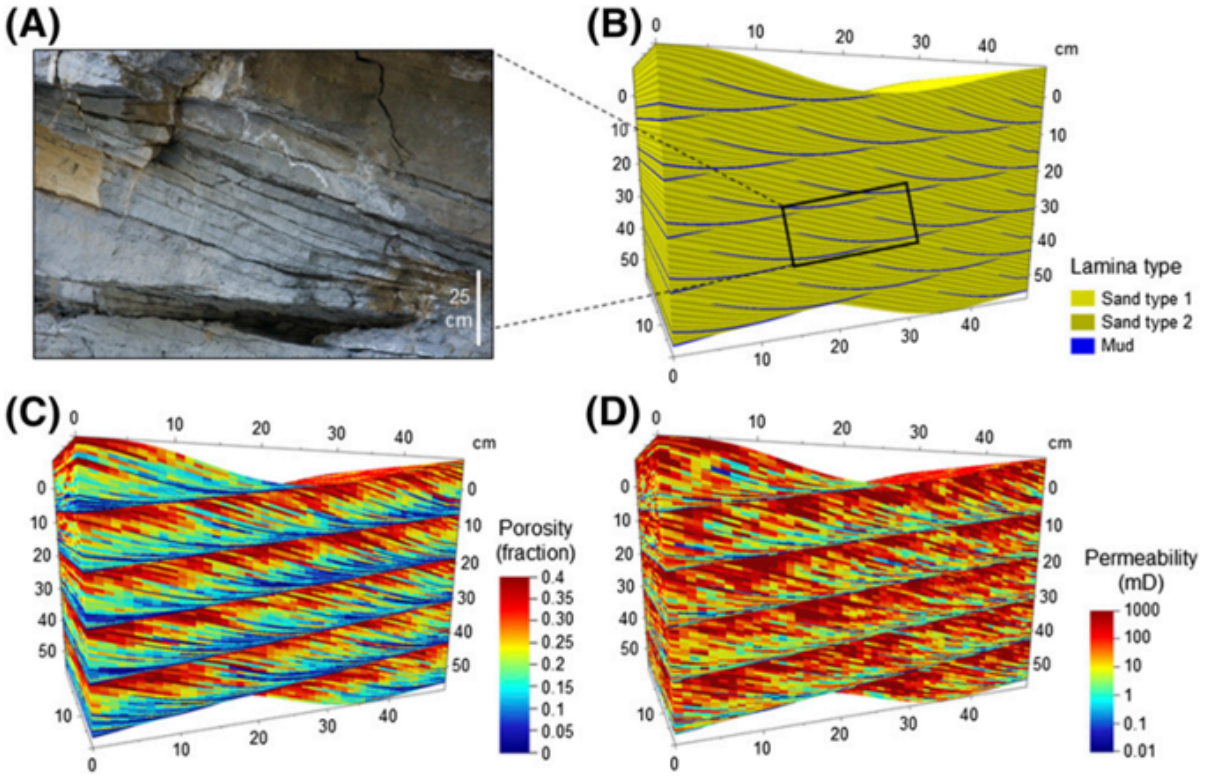

Figure 3.4: (A) Tidal bundles at Isabena Valley. (B) the modeled facies of this exposed unit. (C) and (D) are the porosity and permeability of these tidal bundles (Martinius, 2017)[45].

Lastly, for all non-reservoir facies, very low porosity and permeability values are used. These facies include the prodelta facies, offshore deposits, and marine flooding carbonate deposits.

To summarize all the petrophysical values, namely the porosity and permeability, Table 3.4 represents the values of porosity of each facies, and Table 3.5 represents their permeabilities. These values will be assigned to all geo-models of the Roda Sandstone Formation and used in dynamic modeling.

Table 3.4: The porosity values of each facies that are used in Modeling

Porosity (%)	
Delta-front Sandstone	30
Tidal facies	20
Carbonate-cemented layers	0.1
Prodelta & Offshore facies	0.01

Table 3.5: The permeability values of each facies that are used in Modeling

Permeability (mD)			
Layer	x	y	z
Reservoir	1000	1000	1000
Tidal	500	500	50
Cemented layers	0.001	0.001	0.001
Prodelta & Offshore	1.0E-07	1.0E-07	1.0E-07

4

Methodology

4.1. Procedure of Building the Base Model

This project's geo-models are developed with the utilization of Rapid Reservoir Modelling (RRM), an open-source system of software. This software has been made by Prof.Dr. Sebastian Geiger and his team. RRM is a combination of two real-time and instant sections. These sections are Sketch-Based Interface Modelling (SBIM) and flow diagnostics. When it comes to Sketch-Based Interfaces and Modeling, RRM is a powerful tool. It instantly creates 3D models from 2D drawings mimicking the geologists' traditional approach (pen and paper) in accordance with geologic rules and constraints (for instance, no crossing surfaces). Sketching can be generated in either a cross-sectional window or a map view window. It generates logical models with clearly defined borders between regions represented by surfaces. These surfaces are typically created by the procedure known as Remove Above (RA), Remove Above Intersection (RAI), Remove Below (RB), or Remove Below Intersection (RBI) techniques in the Rapid Reservoir Modeling (RRM) software as shown in Figure 4.1. A details description and elaboration of this method are discussed by Costa Sousa et al. (2020)[46] and Jacquemyn et al. (2021a)[47]. When modeling the Roda Sandstone for this project, we employed the cross-section and map view windows to accurately sketch the Gilbert-delta lobes. These software's windows are seen in Figure 4.2, showing the created surfaces using the aforementioned four techniques (RA, RB, RAI and RBI) following the map view and the cross-section window.

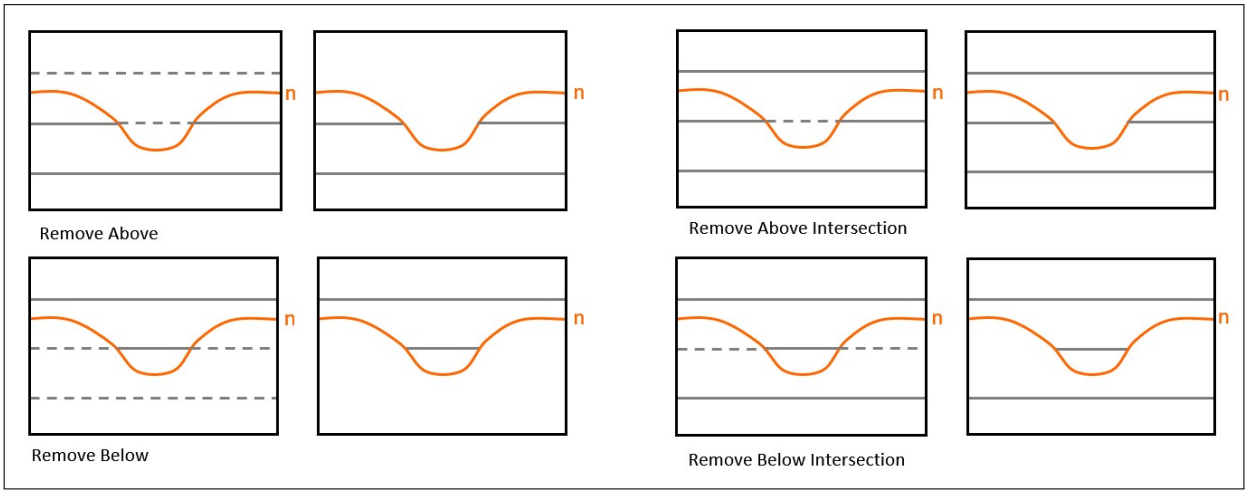

Figure 4.1: Sketching techniques in RRM software (Jacquemyn & Petrovskyy, 2022)[48]

Two examples of this Sketch-based modeling approach with screening assessments of CO2 behavior are conducted by Jackson et al. (2022)[49] and Alshakri et al. (2023)[50].

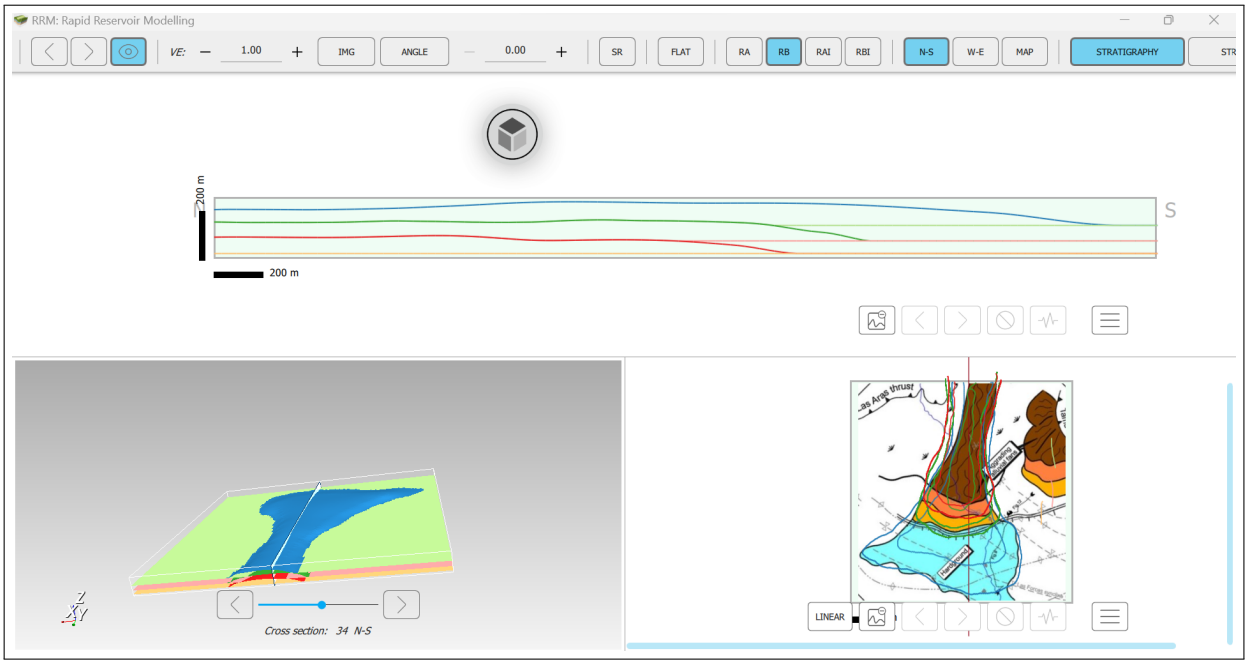

Figure 4.2: A screenshot of surfaces creation using cross-sectional and map view windows in RRM

And the produced surfaces of the Roda Base Model in two perpendicular cross-sectional lines are shown in Figure 4.3.

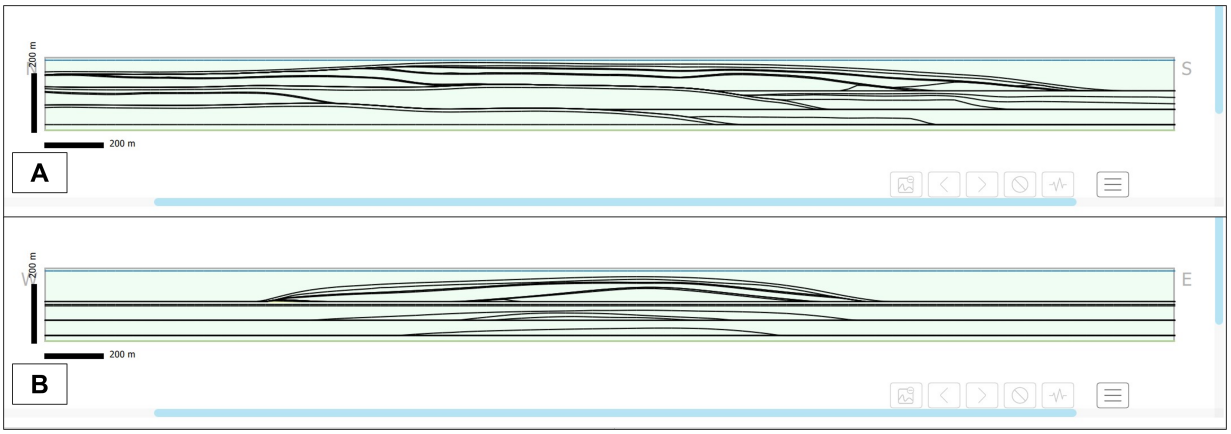

Figure 4.3: (A) N-S cross-section of the generated Roda sandstone surfaces. (B) E-W cross-section

4.2. Techniques for constructing different realizations

To create further realizations, we first select the required regions (the cemented layers) and then apply the four RRM strategies to that part to make adjustments to the carbonate-cemented layers. Following the thin model scenario (scenarios will be discussed in Modeling Chapter), the original cemented layer of the base model has been divided partially to create the thin cemented layers of Model 2. Figure 4.4 shows the new cemented layers and the other part of the split that was added to the main sandstone body.

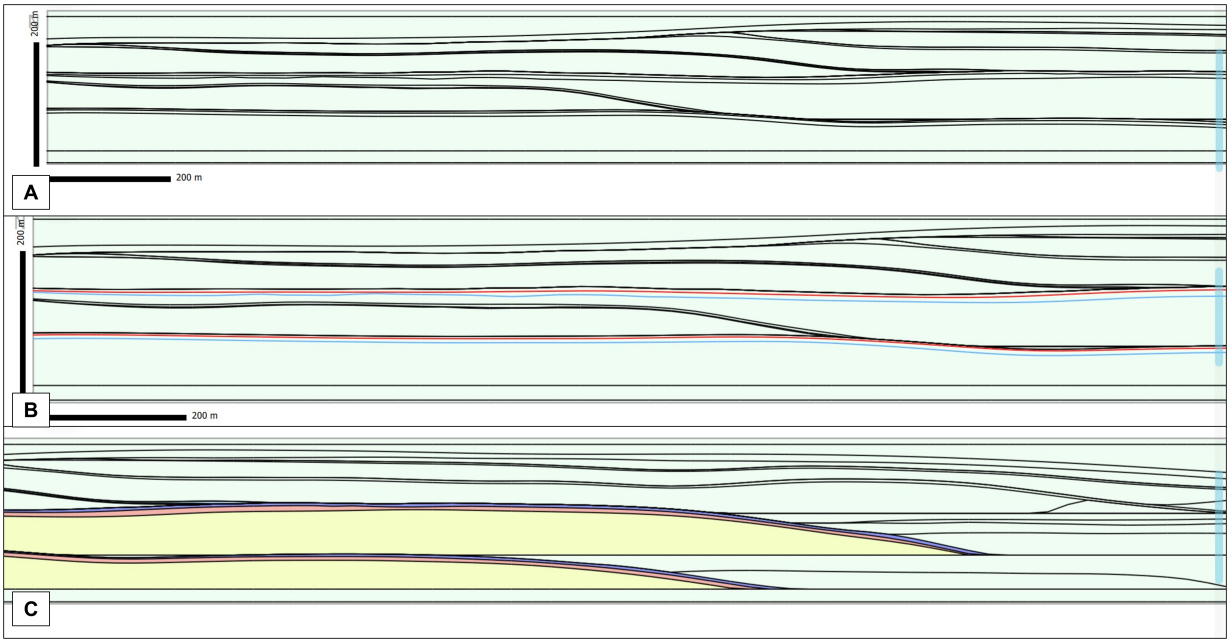

Figure 4.4: Zoomed sections (A) showing the created surfaces for Model 2 with the thin cemented layers. (B) highlights how thin the new cemented layers are with respect to the original cemented layers. (C) the thin cemented layers in the blue and red region are the split part from the original cemented layers and were added to the sandstone body

One of the realizations is to have non-continuous carbonate-cemented layers between the main Roda sandstone lobes and between their sub-lobes. The cemented layers, in this case, were chosen initially, and then their corresponding surfaces underwent modification using the Remove Above Intersection approach such that they now represent patchy cemented layouts as shown in Figure 4.5.

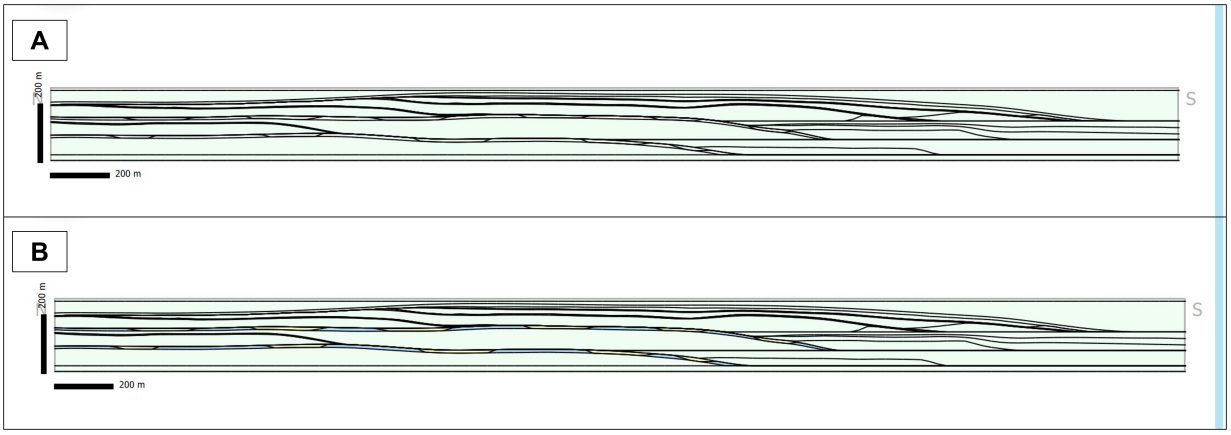

Figure 4.5: (A) How the patchy cemented layers look. (B) the colored patchy cemented layers (blue) and the regions that are split and added to the sandstone bodies.

Similar methods and guidelines were used to construct the other models in this investigation study.

4.3. How the simulator works

The dynamic modeling in this study will be conducted with the usage of the Delft Advanced Research Terra Simulator (DARTS). Dr. Voskov has built this simulator, and he, along with his team, is continuously developing it.

DARTS is comprised of two primary components with regard to its architecture, both of which are essential to the operation of the simulator. DARTS Engine and DARTS Physics are the names of these two parts. The Engine part describes a major part of the governing equations such as Accumulation term, Convection term, Diffusion and Reaction terms, etc. For the Physics part, it is an independent package for each industrial application that will be linked to a particular engine or multiple engines in DARTS and let the simulator to compute all the properties. The connection occurs through either static or adaptive interpolations. It implements the known equations and iterators that the simulator has. When the simulation starts, it computes the first cube by asking properties to compute operator values in each cube corner, and then it uses interpolation. Then, the engine computes the properties of the state and derivatives. Although the simplicity of its architecture and operations, DARTS provides a lot of flexibility. Figure 4.6 displays the architecture of DARTS.

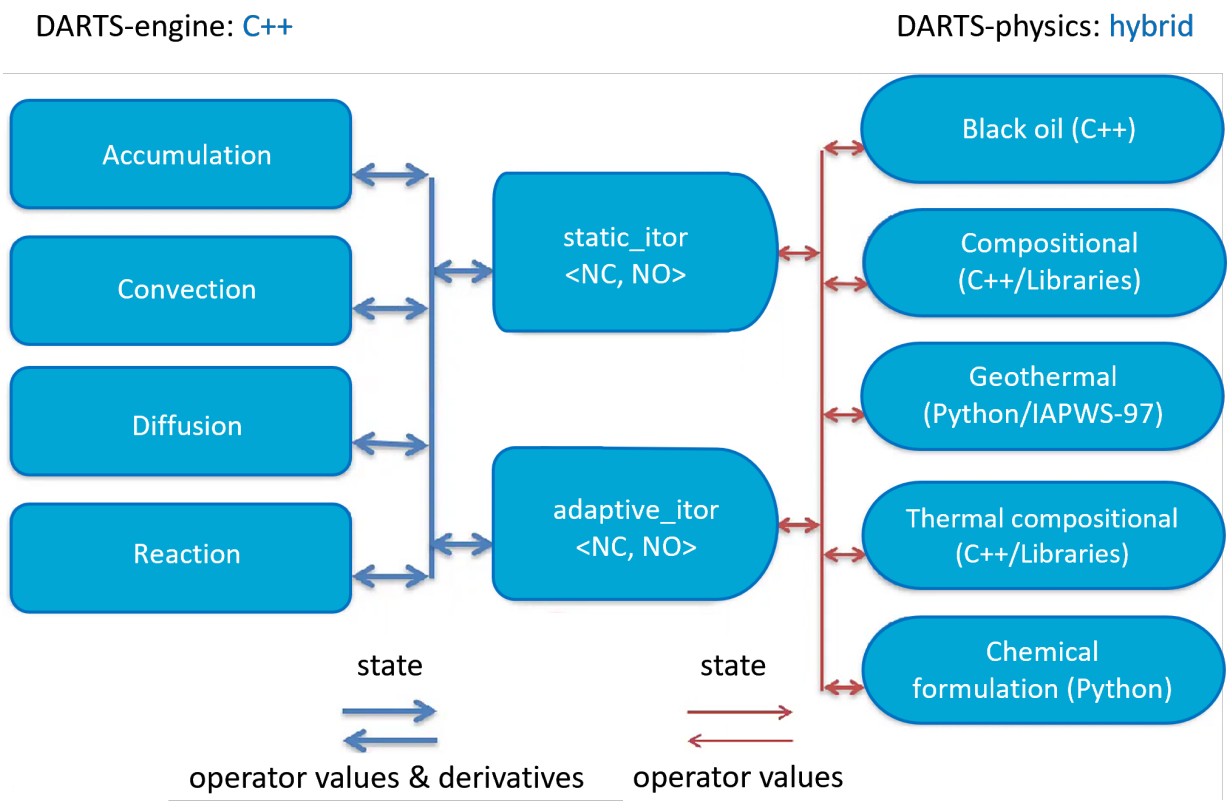

Figure 4.6: The architecture of DARTS

For further information about DARTS, visit the official website of DARTS via: https://darts.citg.tudelft.nl/

4.4. How to assess the simulated models

The obtained dynamic outcomes will be utilized to evaluate the impact of reservoir heterogeneity on the injected carbon dioxide. The assessment will be done through an examination of the CO2 plume's behavior in each model, followed by a comparison of the results. Furthermore, this study will evaluate the effectiveness of each model in relation to subsurface storage, taking into consideration both its capacity and associated risks. The assessment will be addressed in the discussion chapter.

5

Modeling results

This chapter of my thesis report will show and evaluate seven geo-models of the Roda Sandstone formation. These models have been built using Rapid Reservoir Modeling software (RRM). The Roda sandstone facies have been populated in three dimensions by integrating published conceptual models of the Roda Sandstone formation's depositional environment with data from previously logged and established 2D sections from the outcrop. And the thickness and lateral continuity of the carbonate-cemented strata between the three Roda delta lobes (W, X and Y) and their sub-lobes are the fundamental distinctions between these seven models. Each model will be discussed independently in the following sections.

5.1. Base Model

The base model is built upon the geological measurements obtained from the outcrop, as outlined in the datasets chapter. These geological data include the thickness of each layer starting at the bottom with Roda W sandstone followed by its overlaid by a carbonate-cemented layer, then Roda X and Roda Y, respectively, with their carbonate-cemented layers. As an essential aspect of the captured geological data, the continuity of each unit has been appropriately considered. Both the 2D and 3D of each modeled lobe will be shown.

In order to illustrate the laterally propagating changes in the facies, the 2D base model cross-section is shown in Figure 5.1 set in the same dip direction as the Roda sandstone delta lobes towards the SW.

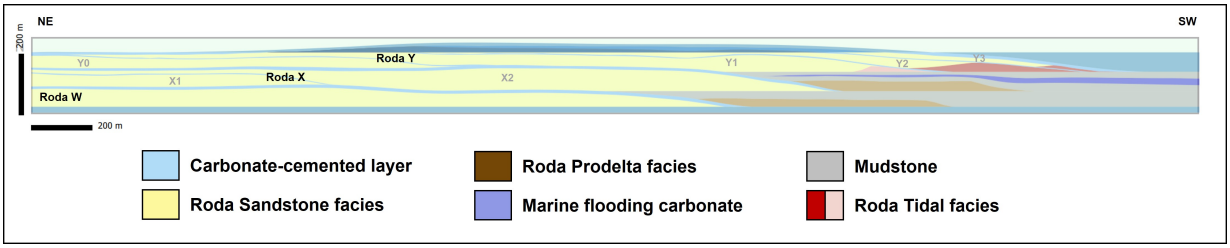

Figure 5.1: NE-SW cross-section of the Roda sandstone base model

The main lobes of Roda W, X, and Y have been vertically stacked, particularly on the landward side. The reason is to investigate the effect of the cemented layers between different models. When comparing Roda X and Y to Roda W, we can see that the latter has the shortest delta lobe. It has one lobe of Delta-front sandstone followed by brown facies, which are bioclastic prodelta deposits. Carbonate then partially cemented the uppermost part of the sand lobe of Roda W as diagenesis (light-blue facies). Before Roda X was deposited, offshore deposits occurred as a transgression in the sequential stratigraphic cycle, followed by the progradation of Roda X. Roda X has two sub-lobes, X1 and X2, and both are cemented at their tops. The marine carbonate facies (dark blue to purple unit) mentioned in the sedimentology section is located between Roda X and Y, where the flooding surface was at its greatest. The largest delta lobe, Roda Y, extends furthest into the sea. It has four distinct sub-lobes labeled Y0, Y1, Y2, and Y3. As a result of Roda Y size, Y1, Y2, and Y3 entered the tidal environments. The models take into account the rock

properties variation between this tidal setting and the delta setting. Lastly, like the previous main lobes and sub-lobes, each Roda Y sub-lobes is cemented by carbonate.

In terms of their 3D architectures, Roda W and X are quite similar to one another, while Roda X is relatively larger. As can be observed in Figures 5.2 and 5.3 for Roda W and Roda X, respectively, both include sandstone deposits as delta-front deposits followed by prodelta deposits and covered by the carbonate-cemented layers. To ensure the capture of the cemented layers in the model, the carbonate-cemented layers are displayed in the grid cells in both figures. Lastly, as was previously demonstrated, the geometry of the delta on Roda Y is atypical. One of the Roda Y sub-lobes (Y2) is seen in Figure 5.4. It is made up primarily of delta sandstone, with tidal deposits appearing towards the distal part of the sub-lobe in the red region. The carbonate-cement unit, which is over the sub-lobe, is another distinctive element that is shown in blue in Figure 5.4 with its shape in the grid resolution.

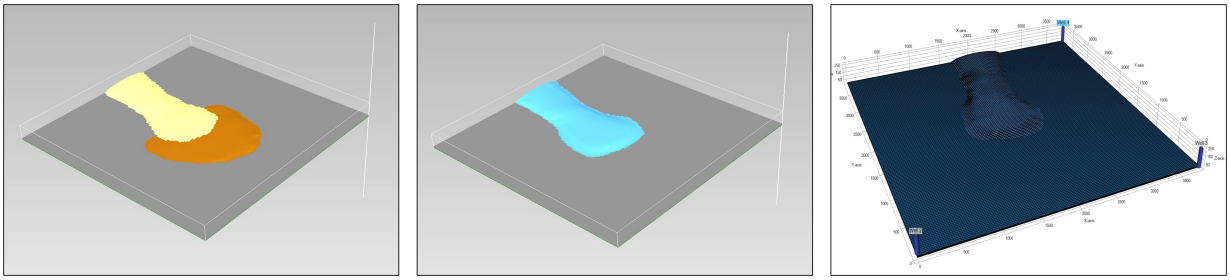

Figure 5.2: 3D model of Roda W. Left: Delta-front sandstone and prodelta deposits, middle: the overlaid carbonate-cemented layer on Roda sandstone, right: the cemented layer with the selected grid resolution

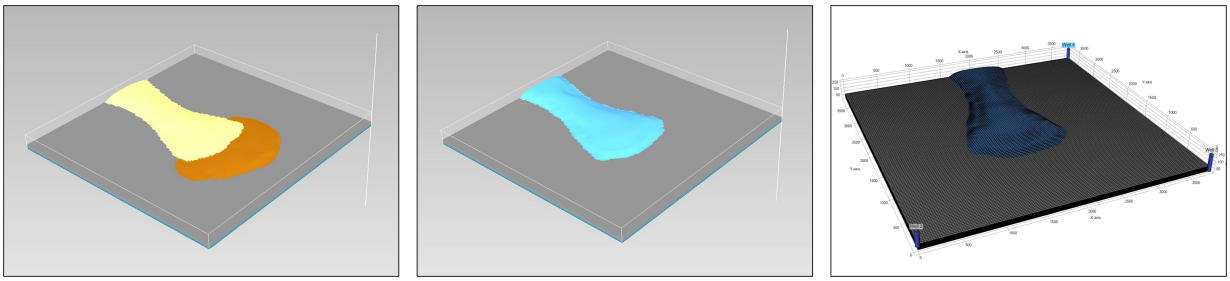

Figure 5.3: 3D model of Roda X. Left: Delta-front sandstone and prodelta deposits, middle: the overlaid carbonate-cemented layer on Roda sandstone, right: the cemented layer with the selected grid resolution

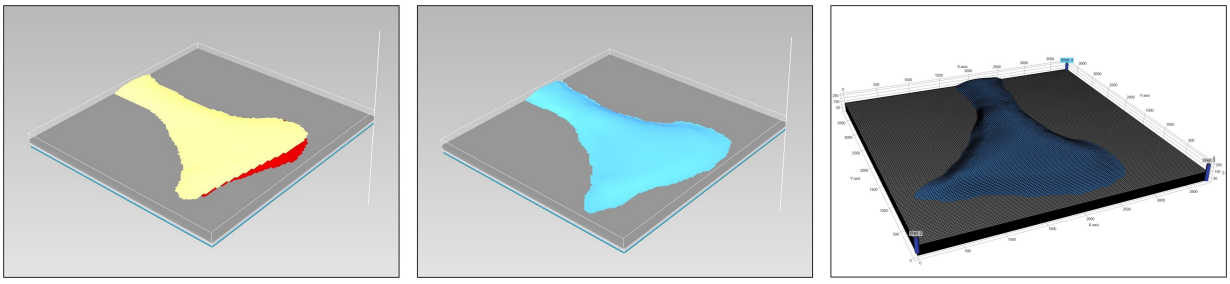

Figure 5.4: 3D model of Roda Y2. Left: Delta sandstone and tidal deposits, middle: the overlaid carbonate-cemented layer on Roda sandstone, right: the cemented layer with the selected grid resolution

The characteristics of the carbonate-cemented layers that are located between the main lobes and the sub-lobes are what distinguish the base model from the other six models and cause it to be regarded as the model that most accurately represents the Roda sandstone formation. As part of this research, the grid resolution of the models has been carefully considered and will be presented in a separate section toward the end of this chapter.

5.2. Model 2

A second model has been constructed with half the thickness of these carbonate-cemented layers between the main lobes and their sub-lobes of Roda sandstone formation in order to more accurately study the impact of reservoir heterogeneity on CO2 plume generation and migration over time. The values of these thicknesses are described in depth in the section devoted to the datasets. A cross-sectional view of the second model in two dimensions is depicted in Figure 5.5.

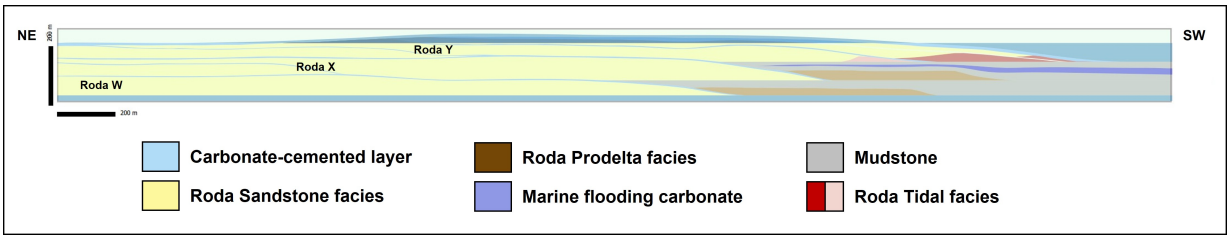

Figure 5.5: NE-SW cross-section of the second model (thin cemented layers) of the Roda sandstone

As compared to the first model, the second model allows us to visualize the variation in thickness of the carbonate-cemented layers as they are significantly thinner in the second model in both main lobes and their sub-lobes of Roda sandstone formation.

The thin cemented layers of Roda W, X, and Y in Model 2 have been mapped in three dimensions, and the results are shown in Figures 5.6, 5.7, and 5.8, respectively, for Roda W, X, and Y2 correspondingly.

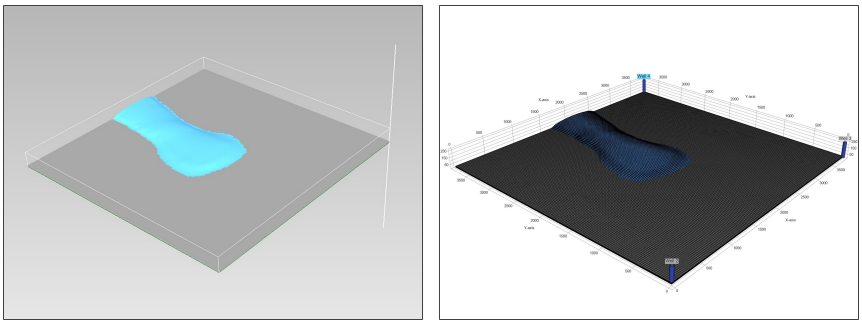

Figure 5.6: Left: 3D carbonate-cemented layer on Roda W sandstone of Model 2, right: the cemented layer displayed in grid cells

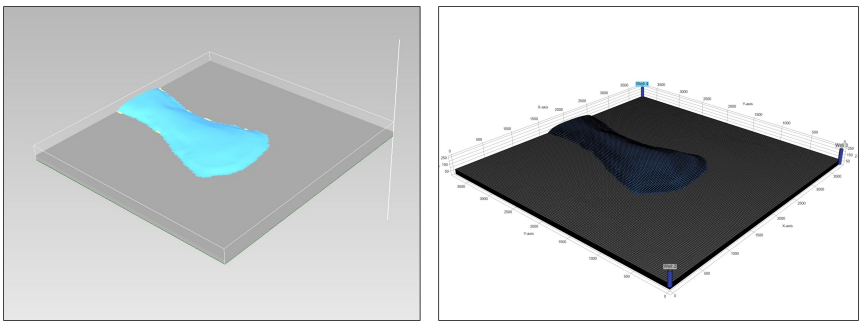

Figure 5.7: Left: 3D carbonate-cemented layer on Roda X sandstone of Model 2, right: the cemented layer displayed in grid cells

It is clear from the 3D figures of Model 2 that the carbonate-cemented layers have been fully captured in three dimensions, despite the fact that they were constructed as thin units. In addition, because of the chosen grid resolution, they are represented in each cell that makes up those layers in Figures 5.6, 5.7, and 5.8, as can be seen.

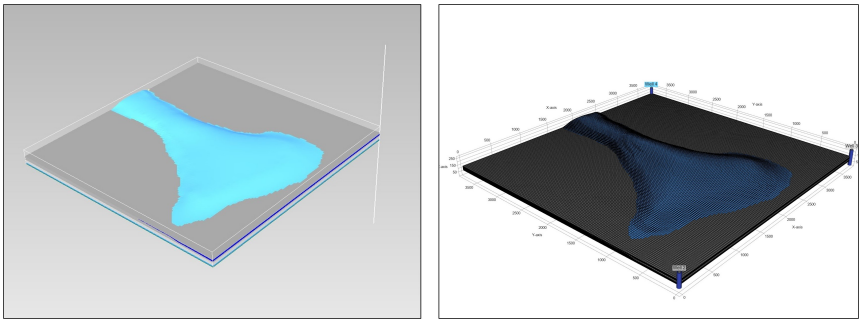

Figure 5.8: Left: 3D carbonate-cemented layer on Roda Y2 sandstone of Model 2, right: the cemented layer displayed in grid cells

5.3. Model 3

Model 3 is built on the same thickness variation assumption as Model 2, with the exception that it includes thick carbonate-cemented strata in between the main lobes and sub-lobes of the Roda sandstone formation. Sandbodies of Roda W, X, and Y maintain the thicknesses that they had initially in the base model, although the thicknesses of these cemented units are doubled in Model 3. This thickness variation can be visibly seen in Figure 5.9.

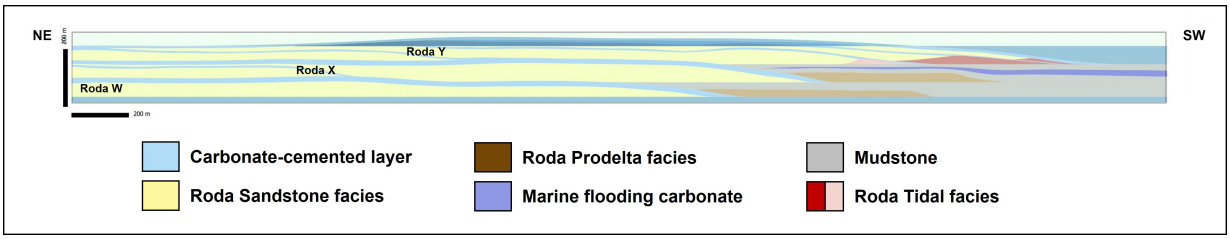

Figure 5.9: NE-SW cross-section of the third model (thick cemented layers) of the Roda sandstone

Additionally, for the purpose of 3D modeling, the thick carbonate-cemented strata that make up each lobe and sub-lobe of the Roda Sandstone Formation have been characterized in all three dimensions. The 3D modeling of Model 3 Included all of the facies, such as delta-front, prodelta, carbonate-cemented, bioclastic marine deposits, and offshore deposits, but for briefness, only the carbonate-cemented Roda W, Roda X, and Roda Y2 units are represented in Figure 5.10.

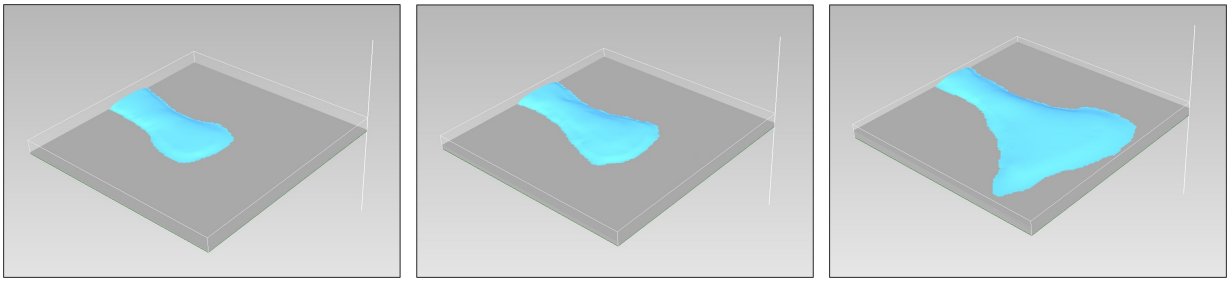

Figure 5.10: The 3D carbonate-cemented layer of Roda W sandstone (left), Roda X (middle) and Roda Y2 (right) of Model 3

Based on the results that Model 3 achieved in its modeling, it is abundantly evident to see that the sand lobes and sub-lobes of Roda W, X, and Y have been efficiently covered by the above carbonate-cemented layers.

5.4. Model 4

The prior models have satisfactorily depicted the thickness changes of the carbonate-cemented strata between the main Roda lobes and their sub-lobes. However, in order to conduct more precise examinations of the influence of these strata on the migration of CO2 plumes, the following models will demonstrate the lateral continuity of these carbonate-cemented layers, preserving their thicknesses at parity with those of the base model. The key component that defines lateral continuity is the degree of cementation and lithification, which in turn depends on the amount of time spent since the cessation of the sedimentation of delta deposits and the availability of carbonate bioclasts.

The assumption in Model 4 is that the carbonate-cemented layer in Roda W did not have sufficient time to reach the full development of the cementation and the lithification. This presumption is depicted in Figure 5.11. In this model, the assumption is also that the carbonate-cemented layers in Roda X and Y remain in the same continuity as the base model.

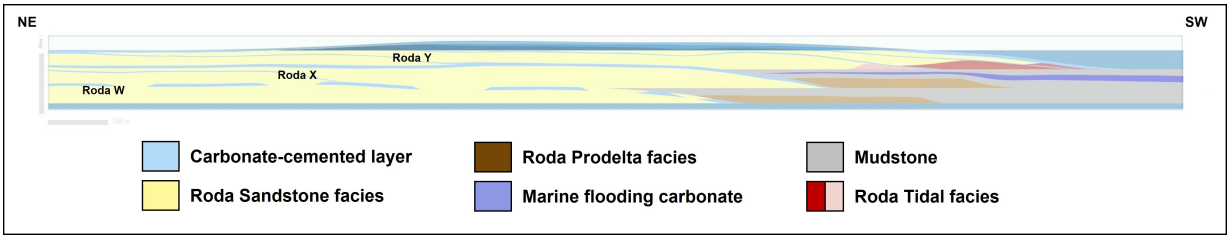

Figure 5.11: NE-SW cross-section of the fourth model (partially cemented of the Roda W lobe)

To visually grasp the patchy degree of carbonate-cementation of Roda W, figure 5.12 shows the 3D model of the modeled layers.

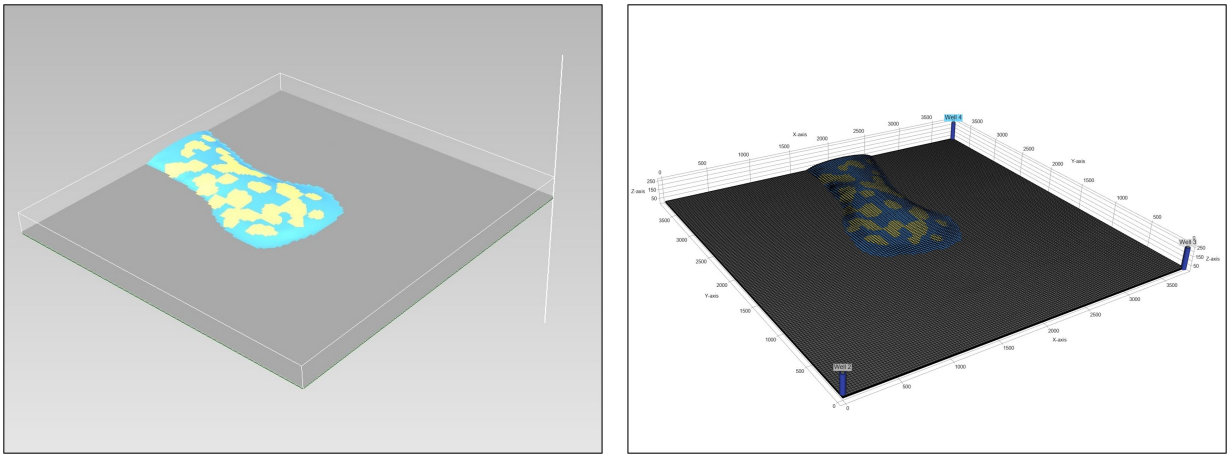

Figure 5.12: Left: 3D partially carbonate-cemented Roda W sandstone of Model 4, right: the cemented layer displayed in grid cells

Figure 5.12 shows that some of the Roda W sandstone (yellow facies) is not covered by the cement layer, indicating the direct contact between the permeable layers of Roda W and Roda X, which may play a role in the vertical movement of the CO2 plume and will be examined in the next chapter.

5.5. Model 5

Model 5, which is based on the same concept as Model 4, investigates the lateral continuity of the carbonate-cemented strata between both the main and the secondary lobes of the Roda Sandstone Formation. Models 4 and 5 both assume that all Roda lobes and sub-lobes are in contact to some extent, but Model 5 goes one step further by also assuming that Roda X and Roda Y have those layers partly cemented in addition to Roda W. The 2D section of this model is seen in Figure 5.13.

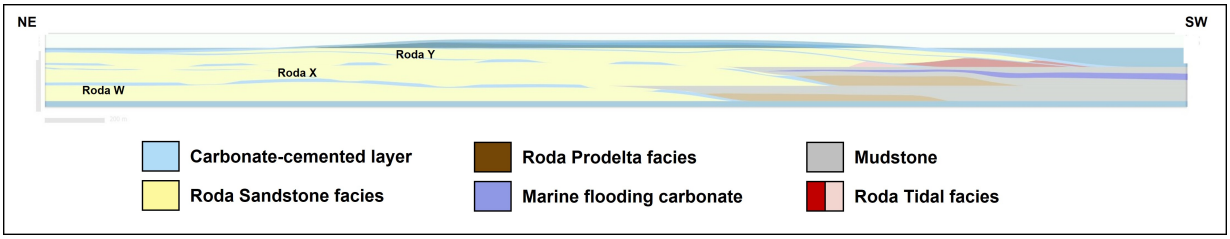

Figure 5.13: NE-SW cross-section of the fifth model (partially cemented of Roda W, X and Y lobes)

Three-dimensional representations of the partly developed carbonate-cemented layers of Roda W, Roda X, and Roda Y2 are presented in blue color in Figures 5.14, 5.15, and 5.16, respectively with their representation in the grid blocks.

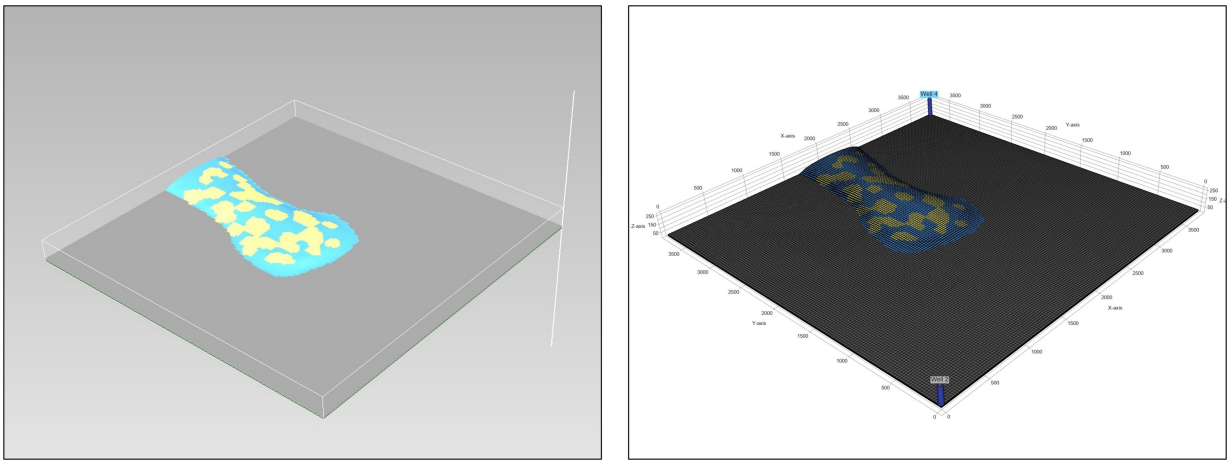

Figure 5.14: Left: partially carbonate-cemented Roda W sandstone (Model 5), right: displayed in grid cells

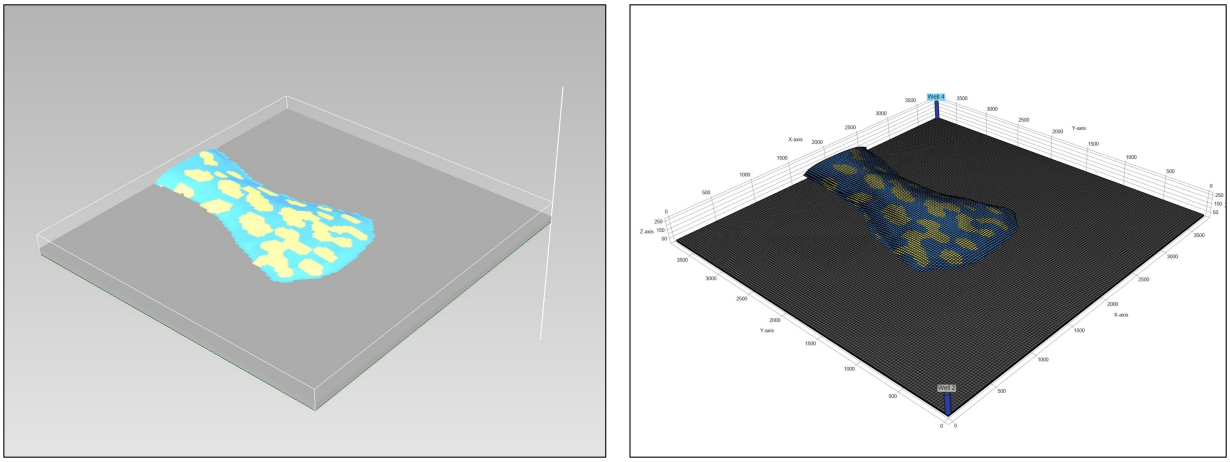

Figure 5.15: Left: partially carbonate-cemented Roda X sandstone (Model 5), right: displayed in grid cells

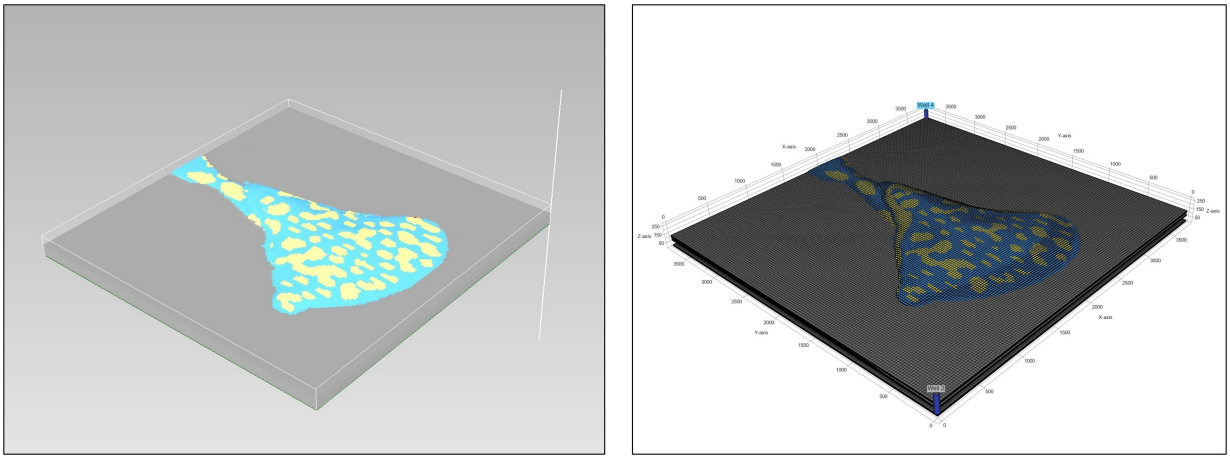

Figure 5.16: Left: partially carbonate-cemented Roda Y sandstone (Model 5), right: displayed in grid cells

5.6. Model 6

Similar to Model 5, but with a longer time for the carbonate cementation process to develop and lithify, but yet not enough to completely cover the Roda sandstone lobes, is Model 6. So, the carbonate cementing results in tighter spacing between layers. In other words, the gaps in the cemented layers are smaller compared to Model 5. The purpose of this model is to observe how well CO2 plume would be migrated over time with smaller holes in the impermeable layers between the highly permeable sandstones. Figure 5.17 shows the cross-section of Model 6.

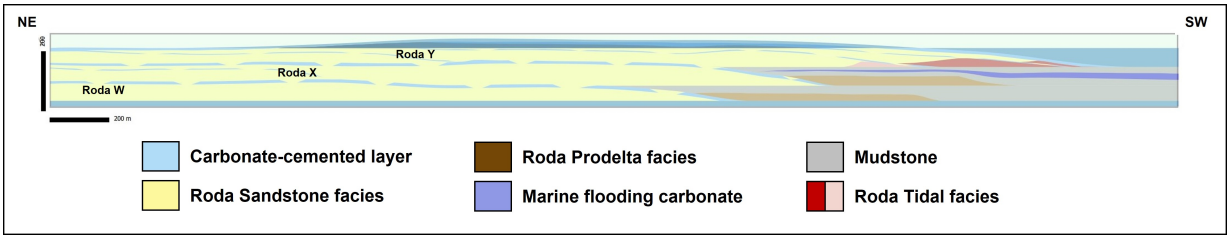

Figure 5.17: NE-SW cross-section of the sixth model (partially cemented of Roda W, X and Y lobes)

To visualize these modeled layers in three dimensions, Figures 5.18, 5.19 and 5.20 demonstrate the small spacing between the carbonate-cemented layers for Roda W, Roda X and Roda Y2, respectively, where we can clearly observe the lateral continuity variations between Model 5 and Model 6.

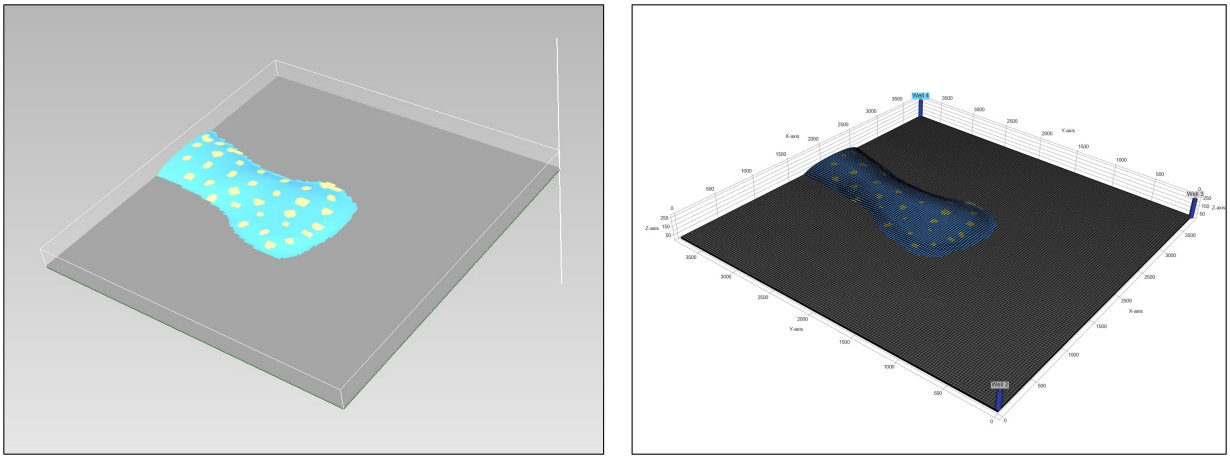

Figure 5.18: Left: partially carbonate-cemented Roda W sandstone (Model 6), right: displayed in grid cells

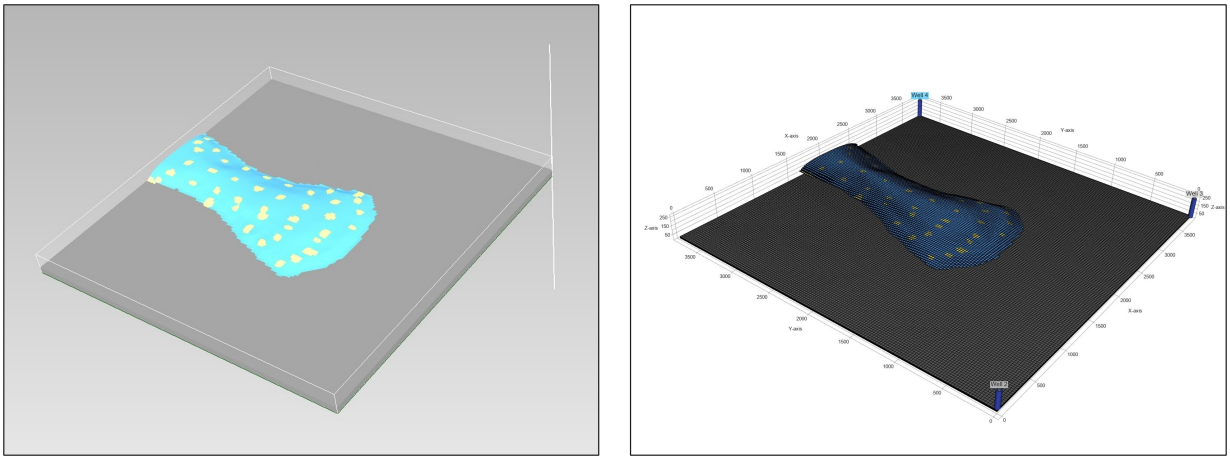

Figure 5.19: Left: partially carbonate-cemented Roda X sandstone (Model 6), right: displayed in grid cells

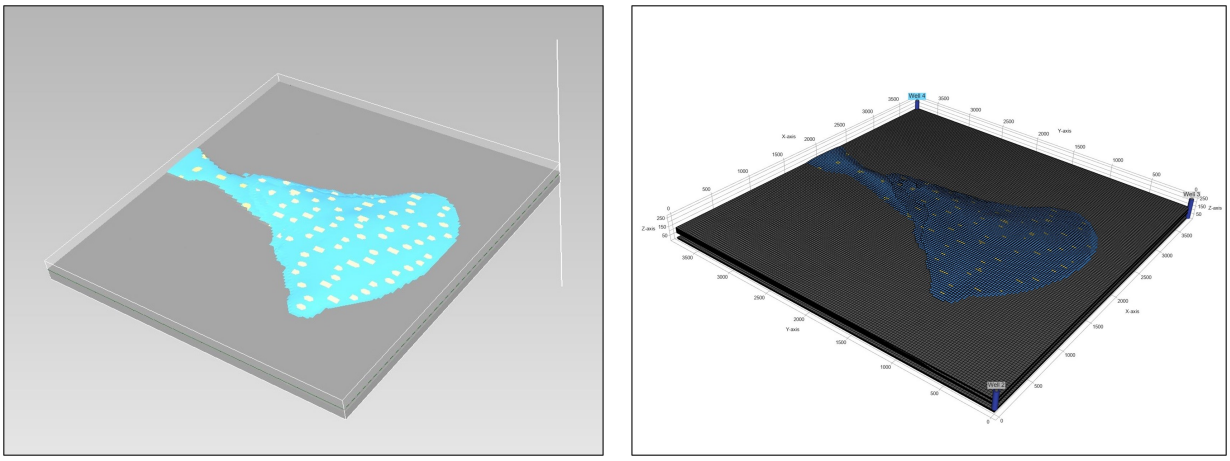

Figure 5.20: Left: partially carbonate-cemented Roda Y sandstone (Model 6), right: displayed in grid cells

5.7. Model 7

In order to gain a more comprehensive comprehension of the impact of reservoir heterogeneity on the migration of CO2 plumes, a hypothetical model has been constructed. Despite the incontrovertible fact that these carbonate-cemented layers were observed and examined in the field, their non-existence is assumed in Model 7, leading to an assumption that the reservoir is homogeneous, which means the Roda lobes and sub-lobes are in contact without any barrier between them. In fact, this model will be beneficial in the investigation of this research. Model 7 is represented in Figure 5.21.

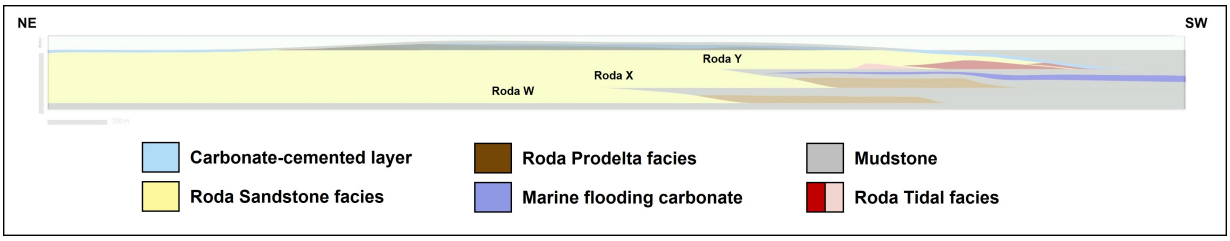

Figure 5.21: NE-SW cross-section of the seventh model (absence of the cemented in Roda W, X and Y lobes)

5.8. Grid Resolution of the Models

Roda Sandstone Formation is represented with sufficient details to allow for reliable conclusions to be drawn on how reservoir heterogeneity—specifically, the carbonate-cemented layers—affects the development and movement of CO2 plumes throughout time. The grid resolution of the models is the measurement of model representation in this project, with higher resolutions representing a more precise model. However, the processing time of the simulator and the computer's capacity to handle these operations set a limit for extremely high grid resolution. Furthermore, after a certain grid resolution, there are no appreciable differences between the model representations.

Various values were tested to determine the best grid resolution for correctly depicting the Roda Sandstone Formation's main lobes and sub-lobes. For briefness, only the Roda Y lobe will be shown in this section. As can be seen in Figures 5.22 and 5.23, the first grid resolution was 21x21x21 in the X, Y, and Z axes, respectively.

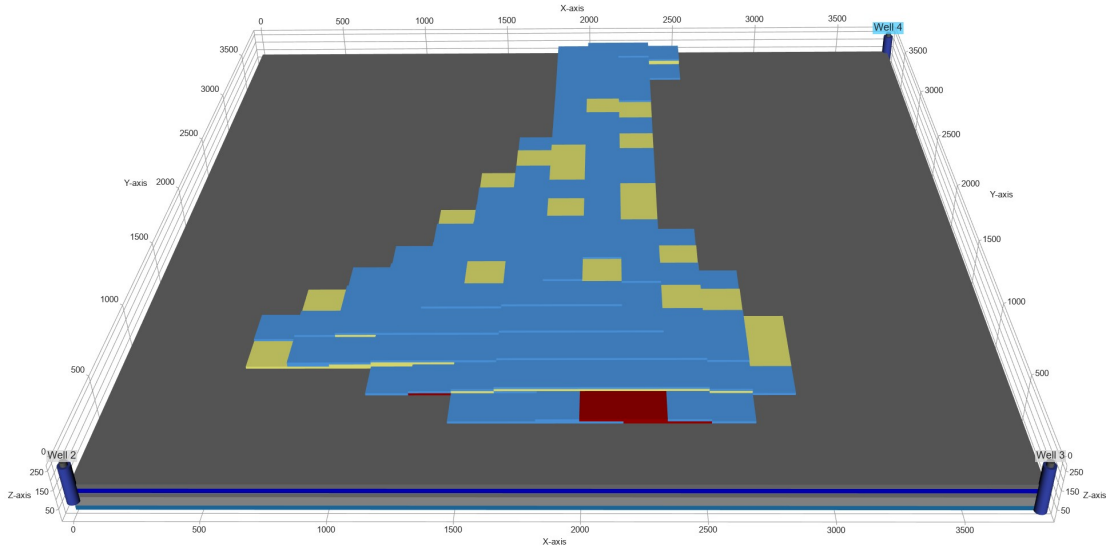

Figure 5.22: Roda Y lobe with a grid resolution of 21, 21 and 21 for X, Y, and Z axes

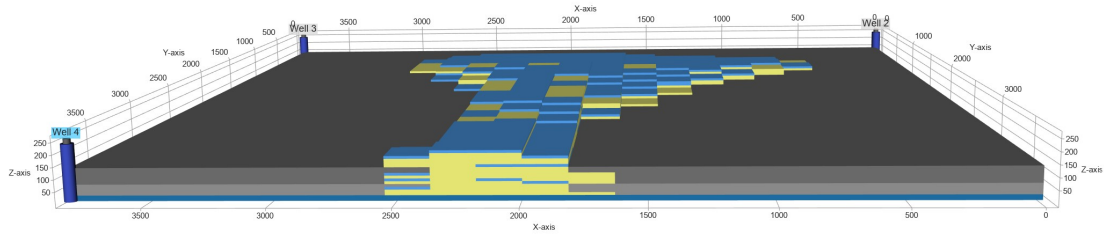

Figure 5.23: The base model with a grid resolution of 21x21x21 from the NE

These two figures prove the inaccuracy of a grid resolution of 21, 21, and 21 on the X, Y, and Z axes, respectively, since the carbonate-cemented layers are not captured in all cells despite their sufficient thicknesses. A higher grid resolution of 41 on the X, 41 on the Y, and 41 on the Z axes was thus evaluated. Figures 5.24 and 5.25 represent the second scenario.

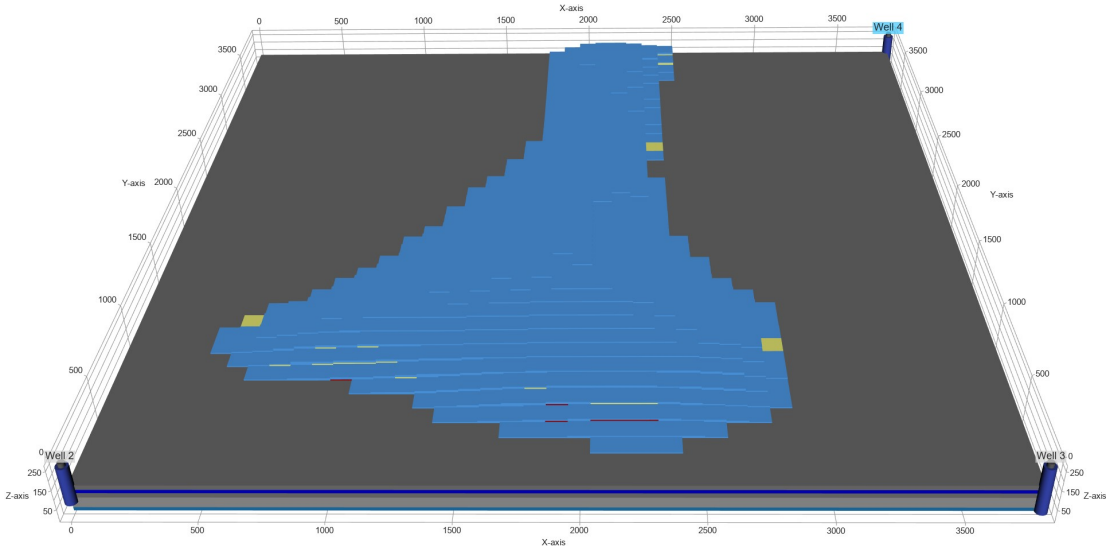

Figure 5.24: Roda Y lobe with a grid resolution of 41, 41 and 41 for X, Y, and Z axes

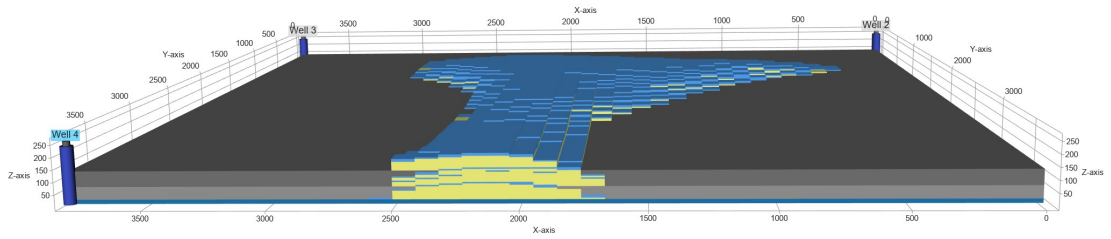

Figure 5.25: The base model with a grid resolution of 41x41x41 from the NE

Yet, the Roda Sandstone Formation was not accurately represented at this grid resolution (41*41*41), indicating that a third assessment is needed. In the following case, the proposed grid size decreased to half, which means the grid resolution is 81, 81 and 81 for X, Y, and Z axes (Figures 5.26 and 5.27)

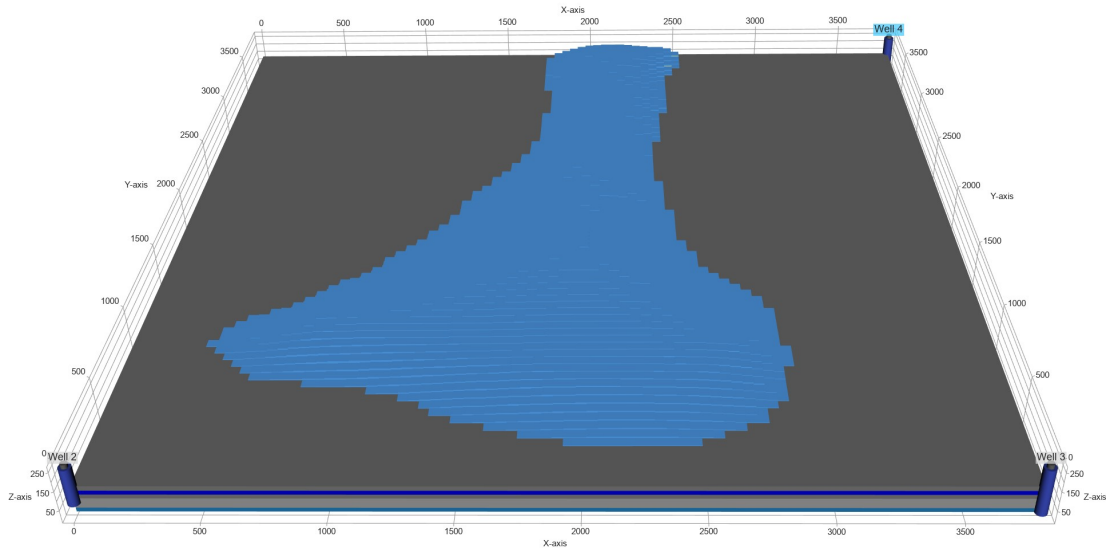

Figure 5.26: Roda Y lobe with a grid resolution of 81, 81 and 81 for X, Y, and Z axes

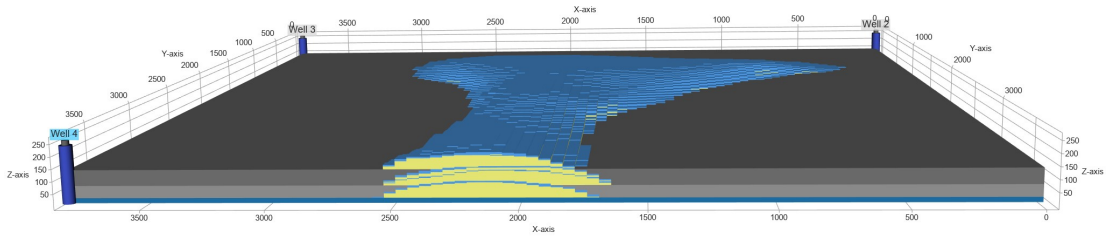

Figure 5.27: The base model with a grid resolution of 81x81x81 from the NE

Despite the fact that the third evaluation of the grid resolution displayed a better representation of the Roda Sandstone Formation than any of the prior cases, a grid refinement still has to be implemented in order to properly depict the characteristics of the small sub-lobes. The X, Y, and Z grid resolutions have been updated to 151, 151, and 235, respectively. Figures 5.28 and 5.29 show the final refinement.

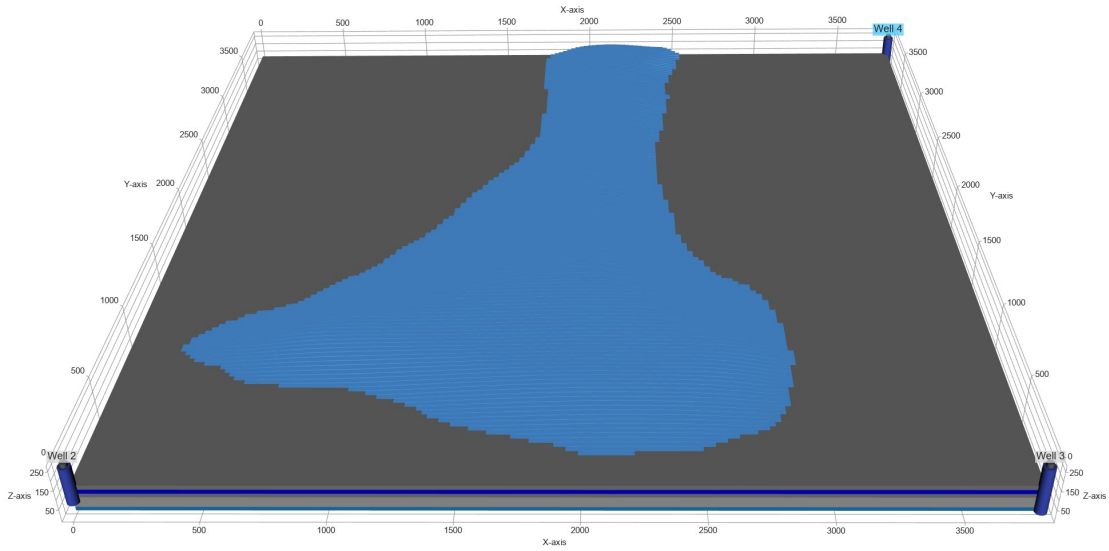

Figure 5.28: Roda Y lobe with a grid resolution of 151, 151 and 235 for X, Y, and Z axes

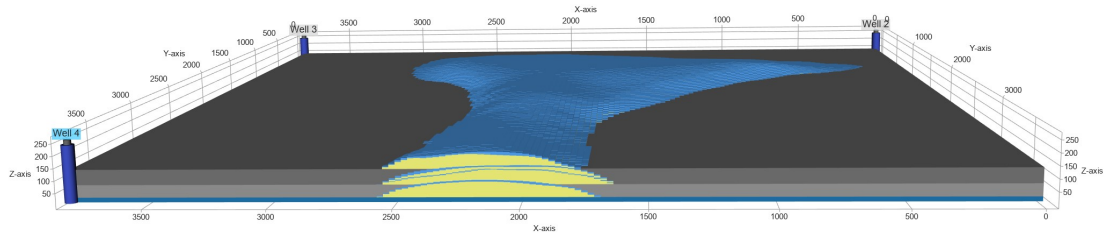

Figure 5.29: The base model with a grid resolution of 151x151x235 from the NE

When evaluating all of the outcomes, the grid resolution of 151 on the X, 151 on the Y, and 235 on the Z proved to be the most accurate representation of the Roda Sandstone Formation. Therefore, it has been selected as the grid resolution of this project's models for dynamic modeling.

6

Dynamic Modeling ”Simulation”

This chapter presents the outcomes of 50 years of dynamic modeling of CO2 injection into the modeled reservoir. These results involve all the models that were previously discussed in the preceding chapter. The dynamic modeling simulator employed in this study is DARTS (Delft Advanced Research Terra Simulator). In addition, this chapter will provide an overview of the dynamic parameters, initial conditions, and the location of the injector.

6.1. Initial Conditions and Dynamic Parameters

The injected CO2 is assumed to be in a supercritical state. This means CO2 behaves as gas-like in terms of viscosity and liquid-like in terms of density (Doughty et al., 2001[51]; Al-Khdheeawi et al., 2017[52]). The applied dynamic parameters in the simulator (DARTS) are:

Dynamic Parameter	Value
Pressure gradient/m	0.1
Initial Pressure (bar)	200
Gas Density (kg/m3)[53]	500
Water Density (kg/m3)	1000
Gas compressibility	1.00E-04
Water compressibility	1.00E-05
connate water saturation (Swc)	0.1
residual saturation (Sgr)[54]	0.07
Injection Rate (m3/day)	4000

Since Roda Sandstone is an outcrop, the assumption is made as it starts at 2000 m deep in the subsurface. This assumption is necessary to utilize the subsurface dynamic parameters during the simulation. The depth of the models can be seen in Figure 6.1

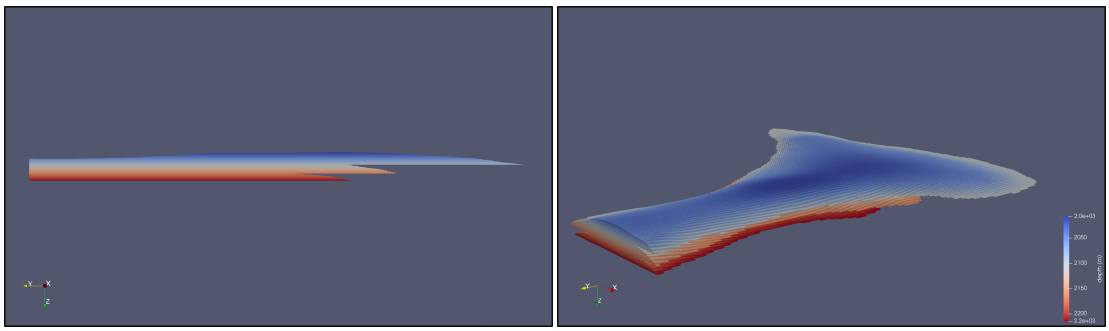

Figure 6.1: The assigned depth in each model in meter in 2D section (left) and 3D (right)

The reservoir is assumed to have an initial pressure with a pressure gradient of 0.1 bar per meter. Accordingly, the pressure gradient with depth in the reservoir is used to illustrate the pressure distribution in Figure 6.2. The initial pressure ranges from 200 bar at top to 223.5 bar at the bottom.

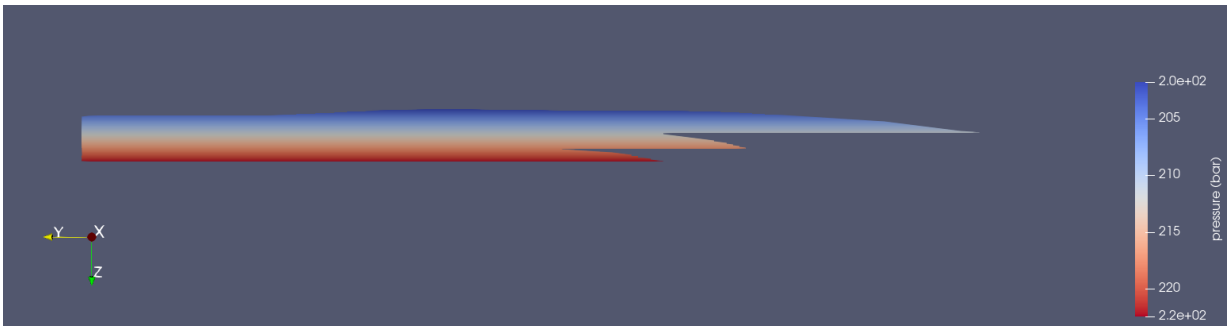

Figure 6.2: The initial pressure of the reservoir

The injection rate is chosen on the basis of the pressure-controlled capabilities. The fracture limit, which is 30% greater than the initial reservoir pressure, was used to regulate the injection rate in the baseline simulation. During this test, the average injection rate was 40.000 m3/day. This test allowed us to determine the maximum safe injection rate for this model. As a result, we settled on a daily injection rate of 4,000 m3.

6.2. Well Location

The placement of the well is selected carefully. The injector is placed in the midst of the Gilbert-delta lobes, such that it could reach all of the Roda Sandstone lobes' major bodies in both the X and Y directions (Fig. 6.3). And for the perforation, the well penetrated all the Roda layers (Roda W, X and Y), as shown in Figure 6.3.

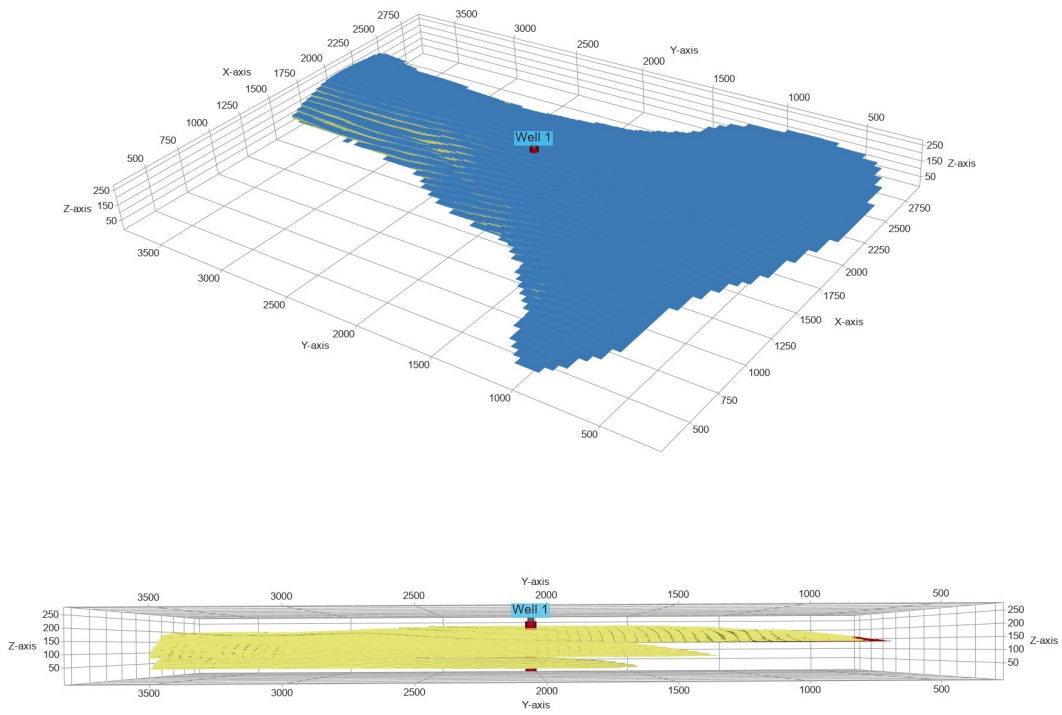

Figure 6.3: The location and penetration of the well through all lobes

6.3. Base Model

The porosity model of model 1 is displayed in Figure 6.4. The non-porous carbonate-cemented layers are shown in blue color and the tidal facies are shown in white, where the main reservoir is displayed in red.

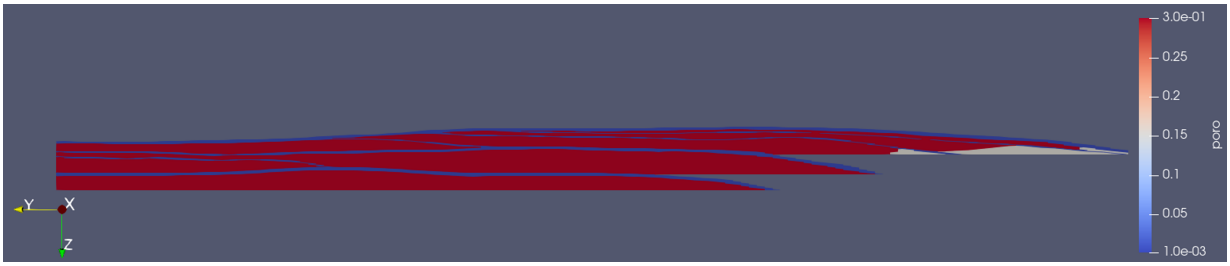

Figure 6.4: sectional view of the porosity values of model 1

Model 1's dynamical outcomes from CO2 injection are shown in Figure 6.5. The figure shows the progress of the injection before and after starting the injection. The results clearly demonstrate that the CO2 plume raised vertically and then migrated laterally when it encountered an impermeable layer.

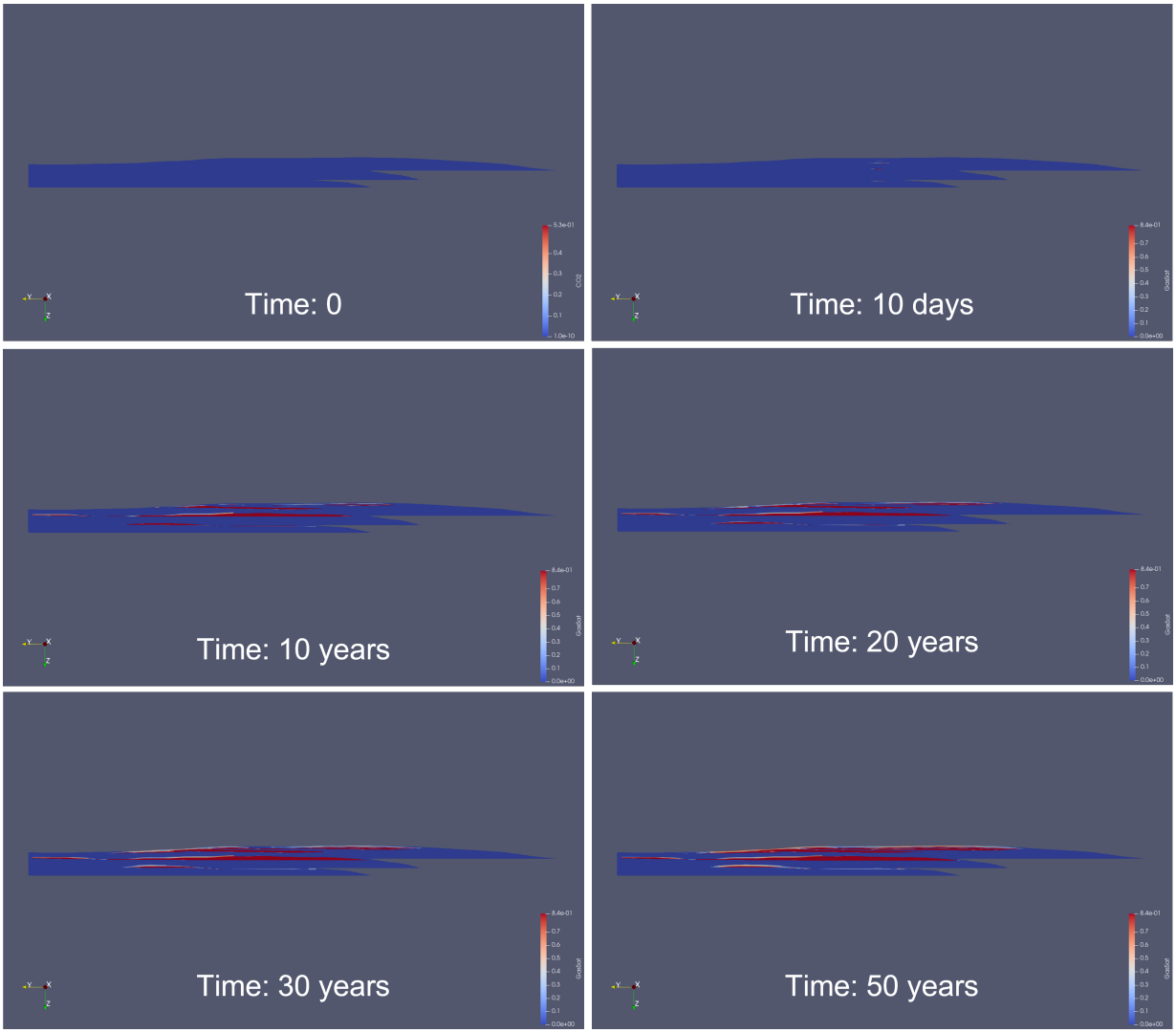

Figure 6.5: CO2 saturation in Roda Sandstone reservoir over 50 years in model 1

The injected CO2 was spread out throughout all three lobes of Roda. Furthermore, the saturation level rose throughout the years, as we can see at 50 years. It's worth noting that since there is no structural trap, the plume reached the reservoir boundaries quickly. Model 1 has an estimated pore volume of 90.02 million m3 as reservoir portions are shown in the porosity model in Figure 6.4. However, we can see that only the upper parts of the Roda lobe bodies are being filled with the injected CO2. For the bottomhole pressure (BHP) of the injection well, it reached a steady state after 25 years with a BHP of 208.3 bar as shown in Figure 6.6.

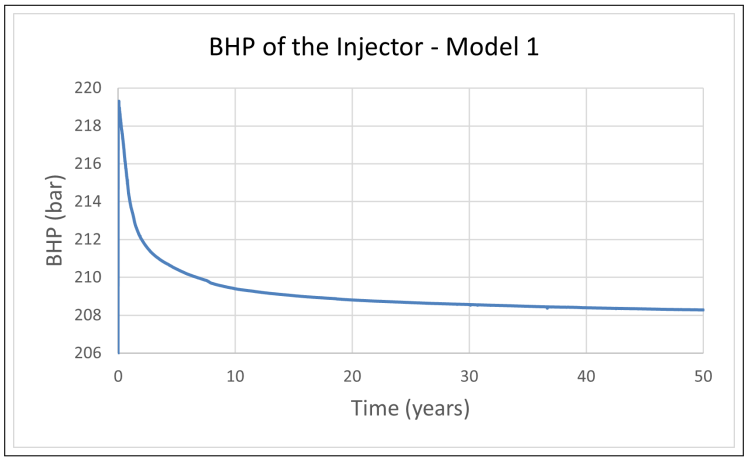

Figure 6.6: Bottomhole pressure (BHP) of the injector over 50 years in model 1

6.4. Model 2

The second model, made up of thin carbonate-cemented layers, has a larger pore volume than the first model, estimated at 96.27 million m3. Dynamic modeling results from DARTS are shown in Figure 6.7.

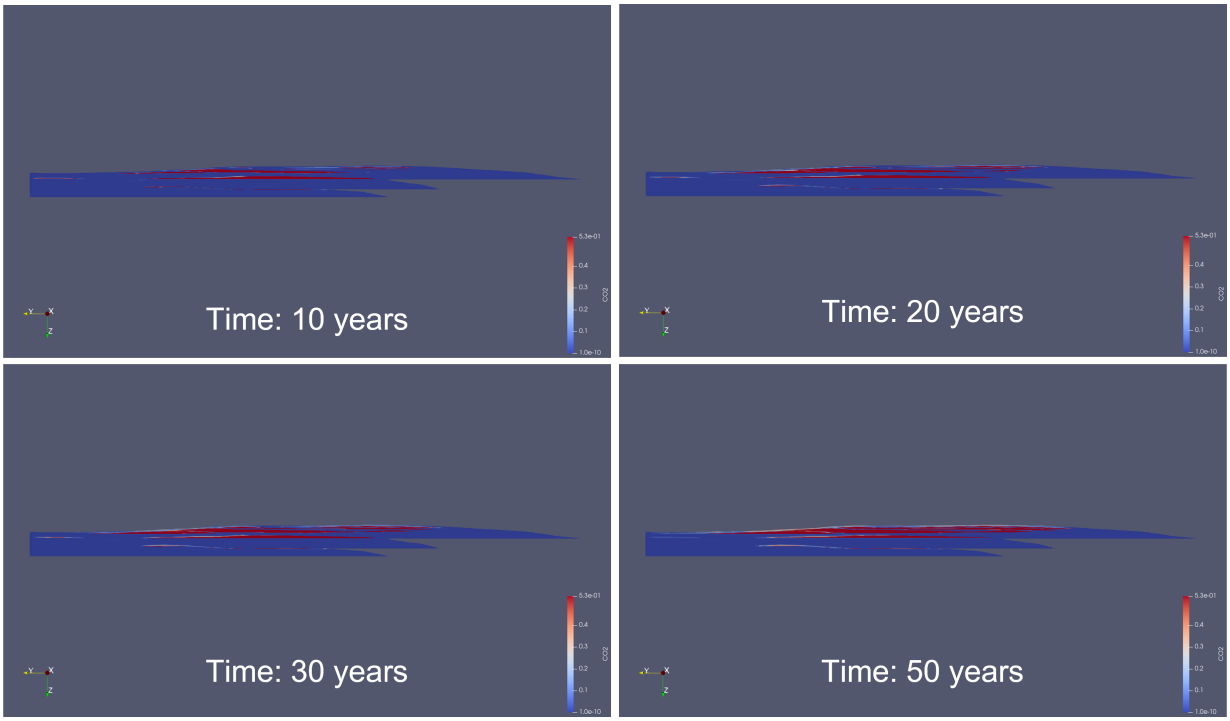

Figure 6.7: CO2 saturation in Roda Sandstone reservoir over 50 years in model 2

Although the carbonate-cemented layers are thinner than the base model, the CO2 plume behaved the same, it rose and then distributed along the impermeable layer in each Roda lobe. With time as we can see the difference between 10 years and 50 years, CO2 plume accumulated and stagnated. As a result, bottomhole pressure (BHP) measurements reveal that after 25 years, the injection well had stabilized at a BHP of 207.3 bar (Figure 6.8).

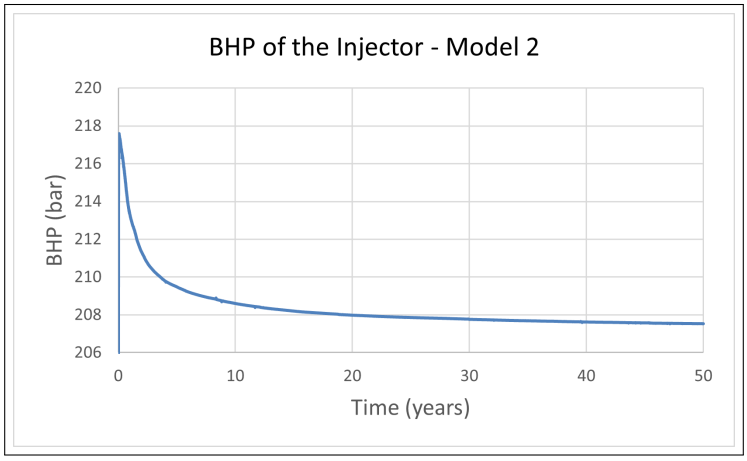

Figure 6.8: Bottomhole pressure (BHP) of the injector over 50 years in model 2

6.5. Model 3

The third model accounts for the presence of the thick carbonate-cemented strata. As shown in Figure 6.9, the behavior of the CO2 plume was comparable with previous models; however, the thick cemented layers shifted the plume's direction slightly toward the NE, and the reservoir became smaller significantly in the upper sub-lobes of Roda Y, making the injection of CO2 relatively challenging, where we can see the faint of the CO2 saturation. It's worth mentioning that the pore volume in this model is around 76.42 million m3.

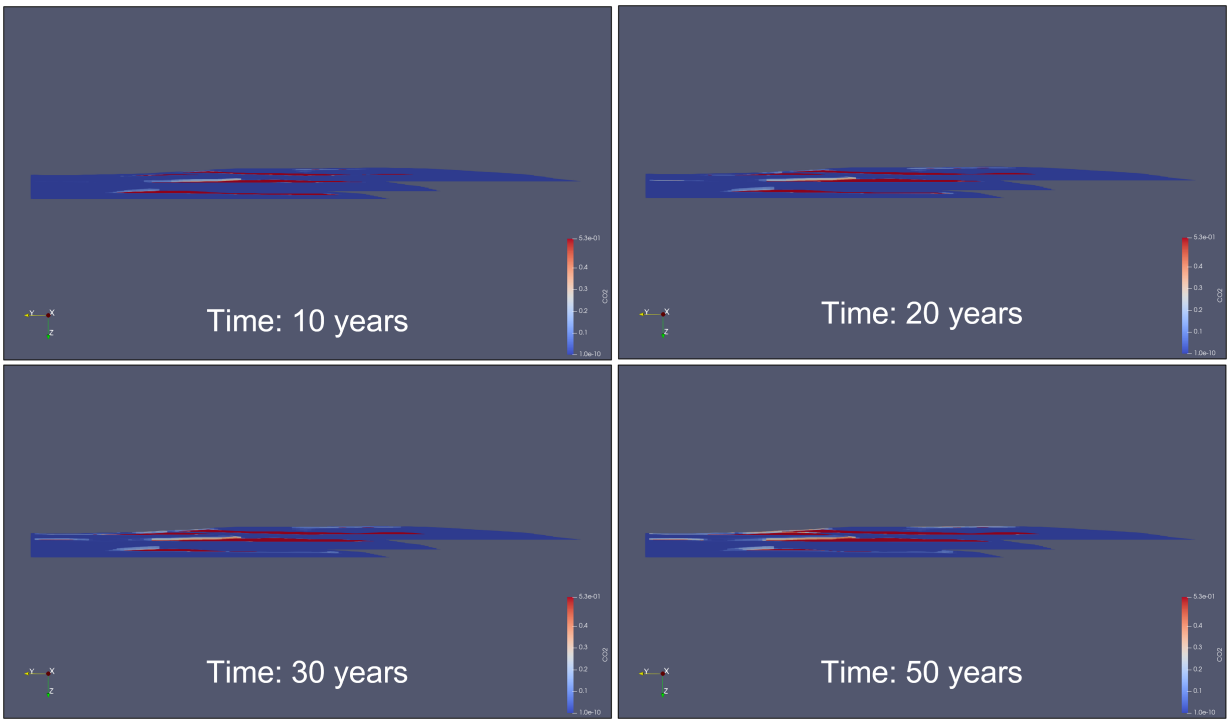

Figure 6.9: CO2 saturation in Roda Sandstone reservoir over 50 years in model 3

The BHP of the injector in the third model reached a steady state after 35 years with a value of 209.6 bar, which is the highest BHP among all models as can be seen in Figure 6.10.

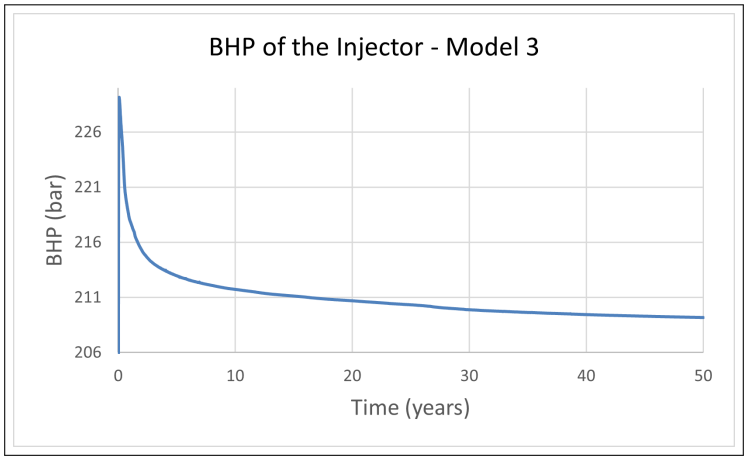

Figure 6.10: Bottomhole pressure (BHP) of the injector over 50 years in model 3

6.6. Model 4

Model 4 comprises the first patchy cemented layers. In this model, the lobes of Roda X and Y, as well as their sub-lobes, are laterally continuous, but only Roda W has the type of cement. The 50-year CO2 plumes in this model are shown in Figure 6.11. Since there is no continuous barrier in Roda W, it is obvious that the CO2 plume did not settle there but instead flowed vertically from Roda W to Roda X. The CO2 plume in Roda Y also followed the same trends as expected from the base case scenario. Model 4's storage capacity, assessed at 91.30 million m3, is larger than that of the base model due to the discontinuity of the cemented layer in Roda W.

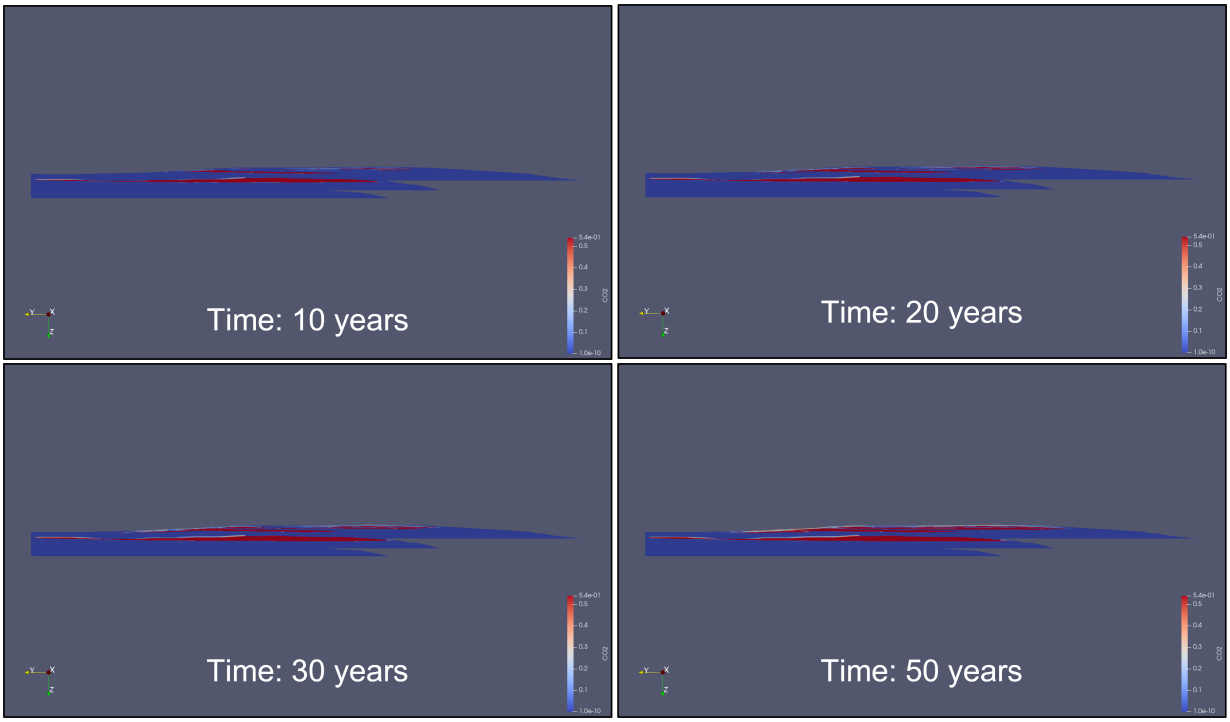

Figure 6.11: CO2 saturation in Roda Sandstone reservoir over 50 years in model 4

Figure 6.12 displays the bottomhole pressure (BHP) of the injection well, which is comparable to but slightly less than that of the basic model (208.2 bar) due to the inclusion of a single patchy cemented layer in Model 4.

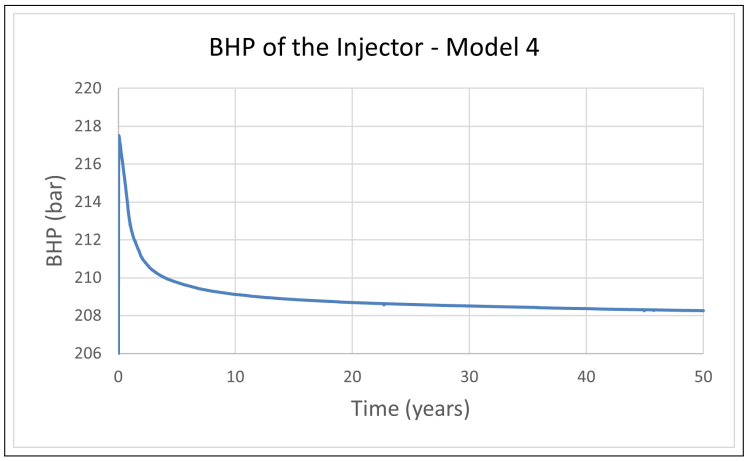

Figure 6.12: Bottomhole pressure (BHP) of the injector over 50 years in model 4

6.7. Model 5

All cemented layers in Model 5 are built of non-continuous patchy cement, allowing for further study of the influence of these cemented layers on the CO2 plume. Figure 6.13 shows a porosity model which includes these cemented layers in Roda W, X, and Y lobes and their respective sub-lobes, where we can see these patchy cemented layers displayed in blue colors between the sand bodies as shown in red color. Indeed, Model 5's cement modeling results in an estimated pore volume of 96.4 million m3, which is more than the pore volumes reported in the previously discussed models.

Figure 6.13: sectional view of the porosity values of model 5

After performing 50 years of CO2 injection into the Roda reservoir, the bottomhole pressure of the injector steadied at a relatively lower value than in any of the prior models after 30 years. This low value is due to the patchy cement layers, where the contact between the reservoir bodies is higher. As shown in Figure 6.14, Model 5 has a BHP of 206.8 bar at steady state.

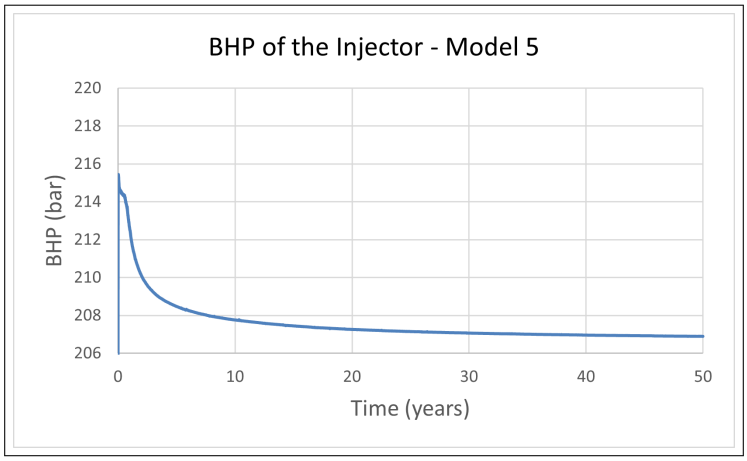

Figure 6.14: Bottomhole pressure (BHP) of the injector over 50 years in model 5

The CO2 plume was able to move vertically through Roda W, Roda X, and the lower sub-lobes of Roda Y because of the patchy carbonate-cemented layers in Model 5. Once the CO2 plume reached the top of the reservoir, where there is a laterally continuous non-permeable layer, it then migrated laterally toward the reservoir boundaries. The dynamic results obtained from DARTS are shown in Figure 6.15. This behavior demonstrates how the patchy cemented layers have the potential to remarkably alter the progression of the plume over time.

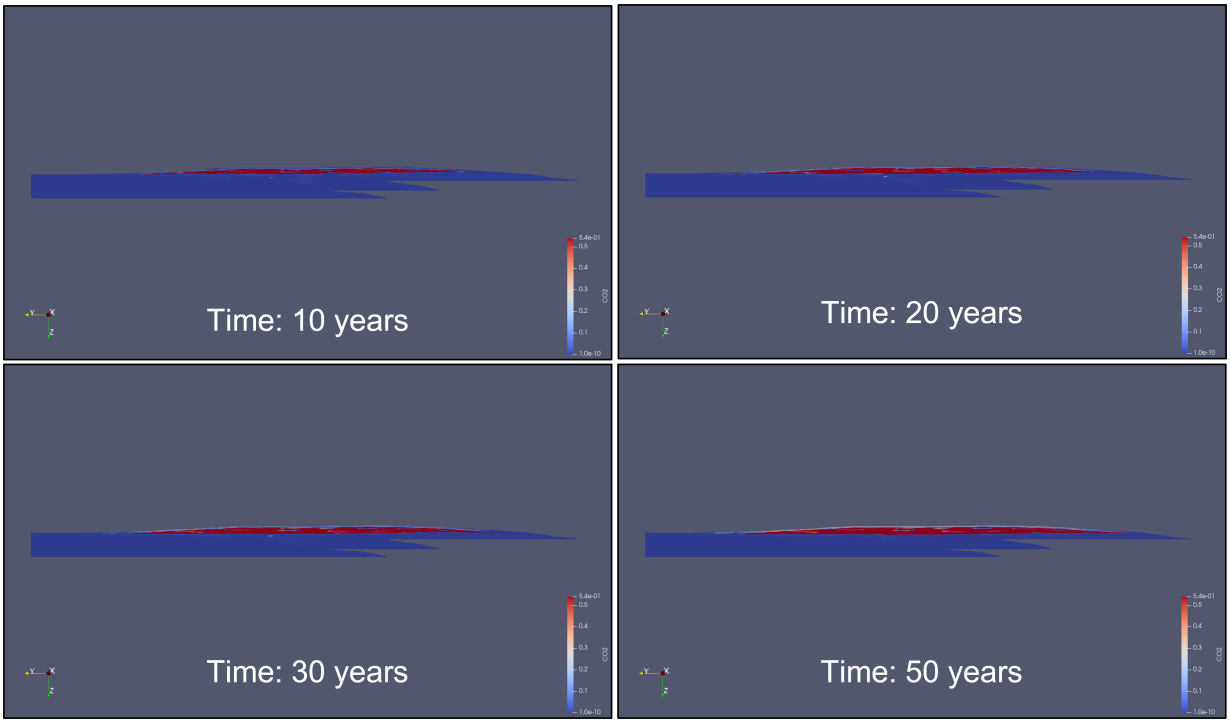

Figure 6.15: CO2 plume in Roda Sandstone reservoir over 50 years in model 5

6.8. Model 6

Model 6 is identical to Model 5, only with tighter gaps between the patchy cement layers. This means that the contact between the sand bodies of the Roda lobes exists but in a smaller size pattern. The results of the dynamic modeling are shown in Figure 6.16. Generally, models 5 and 6 are quite similar in the CO2 plume trend; however, in Model 6, there are additional thin light plumes that are visible in the middle of

the reservoir on Roda X and the sub-lobes of Roda Y. The reason for this behavior is the shape and the spacing between tiny patchy cement layers, which are a low-relief concave-down and close to each other in some areas where they hold some plumes.

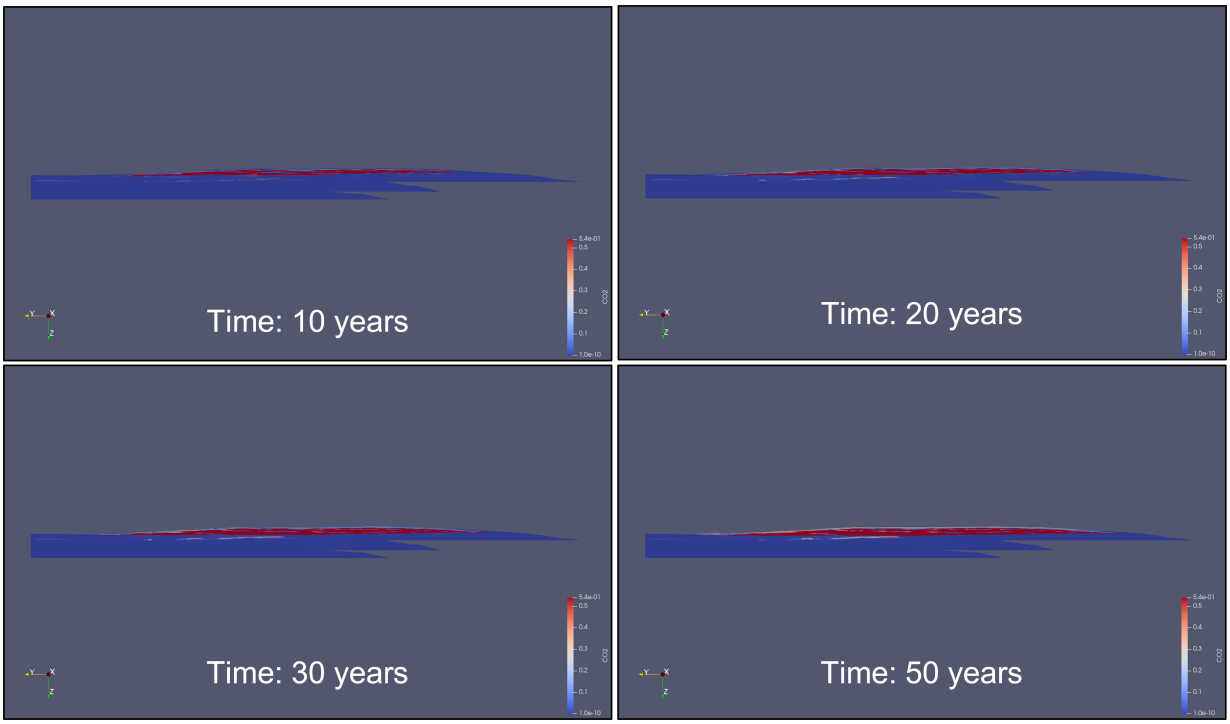

Figure 6.16: CO2 plume in Roda Sandstone reservoir over 50 years in model 6

Correspondingly, the bottomhole pressure of the injector in Model 6 shows a higher value comparably to Model 5, which reflects the influence of the smaller gaps between the carbonate-cemented layers in Model 6. This model has a BHP of 207.05 bar at a steady state, as shown in Plot 6.17.

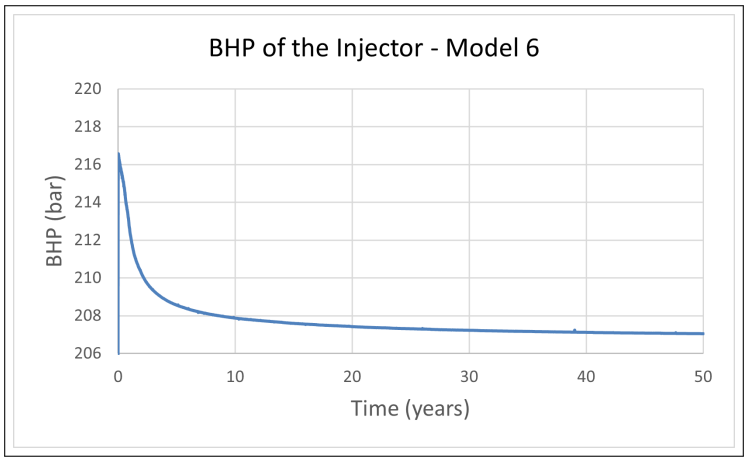

Figure 6.17: Bottomhole pressure (BHP) of the injector over 50 years in model 6

6.9. Model 7

As was discussed in the prior chapter, Model 7 is a homogeneous model of the Roda sandstone since it does not take into account the presence of the carbonate-cemented layers that separate the major lobes and their sub-lobes. To visualize this homogeneous model, Figure 6.18 displays the porosity of this model.

In fact, the lack of cemented layers causes this model to have the greatest capacity among all the models in this study with a volume of 107 million m3.

Figure 6.18: sectional view of the porosity values of model 7 that represents the homogeneous model

When CO2 was injected into the reservoir in Model 7, the plume immediately rose and passed through all the Roda sandstone lobes and sub-lobes and then distributed along the impermeable top seal. After that, it started approaching the reservoir boundaries, as shown in Figure 6.19. In other words, the absence of the cemented layers, which act as impermeable layers within the reservoir, allowed the CO2 plume to accumulate and distribute only in the top part of the reservoir. Furthermore, the plume's behavior and flow exhibit smoothness due to the implementation of the homogeneous model. This can be observed in Figure 6.19, where the plume's shape remains uniform over a period of 50 years, as depicted by the dynamic results.

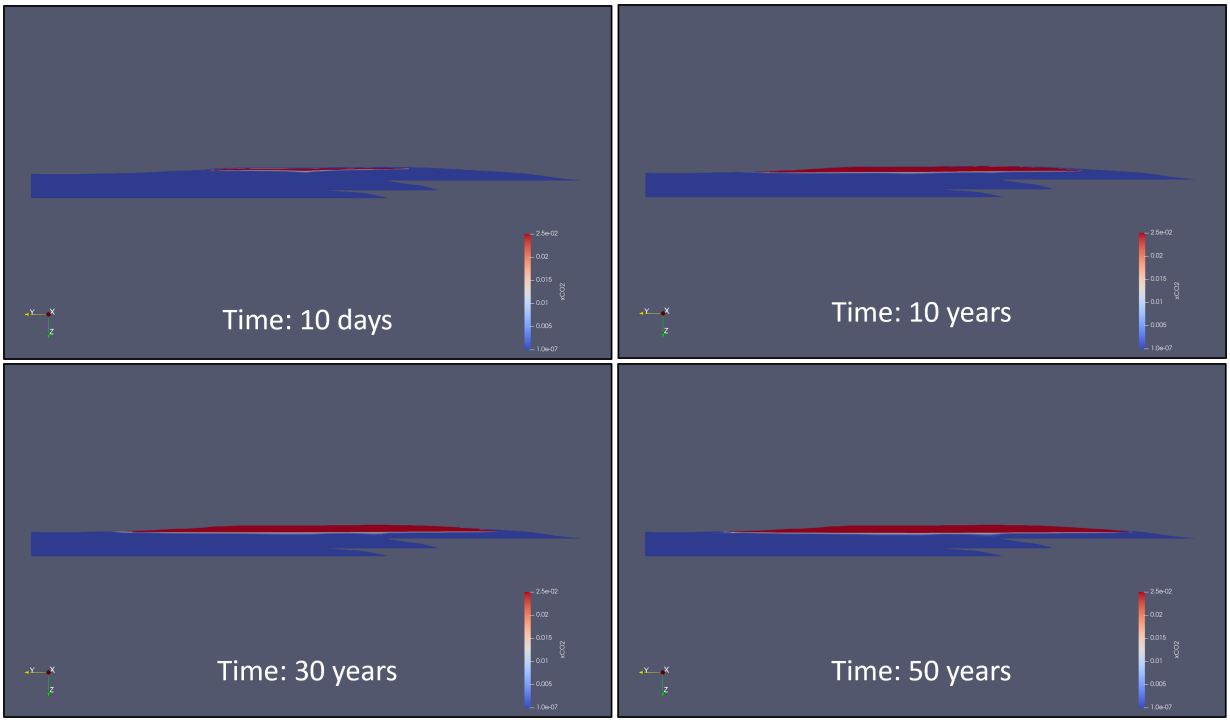

Figure 6.19: CO2 plume in Roda Sandstone reservoir over 50 years in model 7

As a direct consequence of this, the bottomhole pressure of the injector in Model 7 is the lowest of all the models; this is because the lack of carbonate-cemented layers has a significant impact on the value of this parameter. According to the information shown in Plot 6.20, this model has a BHP that is 206 bar at a steady state after 20 years.

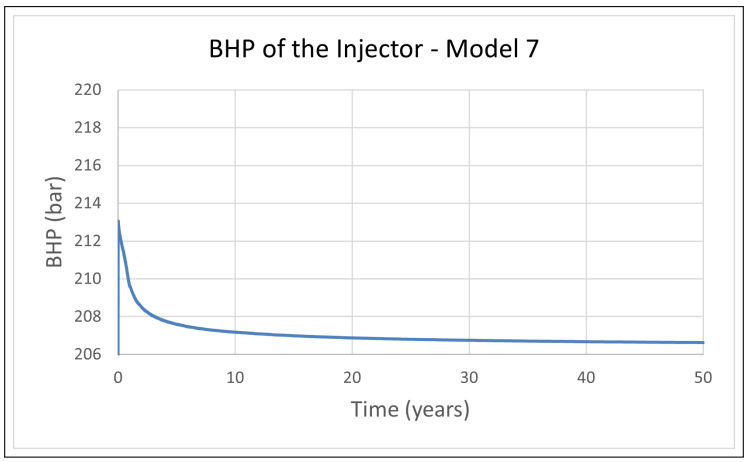

Figure 6.20: Bottomhole pressure (BHP) of the injector over 50 years in model 7

To summarize the results, the bottomhole pressure (BHP) values of all models are plotted in Figure 6.21..

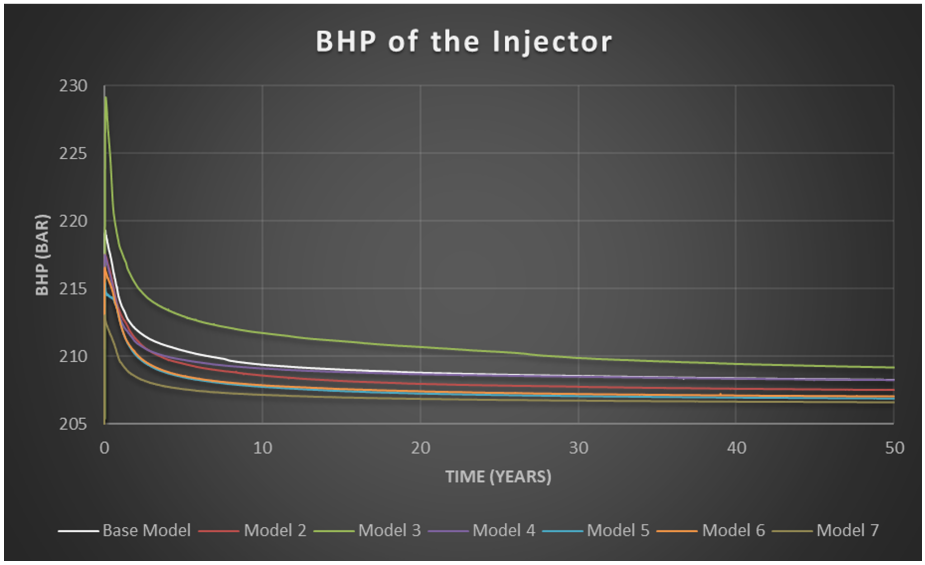

Figure 6.21: BHP of all models in one plot

7

Discussion

7.1. Discussing the results

Upon observing the simulation outputs of the injected carbon dioxide (CO2), it becomes imperative to analyze and address the impact of reservoir heterogeneity, specifically the impermeable cemented layers situated amidst the sand bodies (models' heterogeneities are summarized in table 7.1).

Table 7.1: Summary of the models' characteristics

Model	Characteristics
Model 1	Base model
Model 2	Thin cemented layers
Model 3	Thick cemented layers
Model 4	Patchy cement (Roda W)
Model 5	Patchy cement (all)
Model 6	Patchy cement (tight gaps)
Model 7	Homogeneous

This analysis refers to the development of the CO2 plume and its subsurface storage. The flow direction of the CO2 is dominated by buoyancy, causing the CO2 in the homogeneous rock volume (Model 7) to flow immediately upward from the injection position and bypass much of the homogeneous rock volume, lifting most of the rock volume not used for storage despite the higher pore volume exists. While Models 1, 2, and 3 prove that when the rock volume is heterogeneous with laterally continuous impermeable layers, even with variation in their thicknesses, the flow path of the CO2 plumes gets dispersed, increasing the percentage of the contacting area between the CO2 and the rock volume and consequently, the storage capacity of this buoyant fluid. This is because of having more CO2 volumes in the lower parts of the rock volume as CO2 is distributed along the impermeable layers. In addition, when the reservoir consisted of non-continuous cemented layers between the sand bodies (Models 4, 5, and 6), a considerably higher volume of porosity was accessed owing to the complexity of the flow pathways that the CO2 took regardless of the gap size between the cemented layers. Since there is no structure in these models that traps CO2, the plumes are distributed along the impermeable layers, and the residual trapping is expected to be higher.

Although the injected volume of carbon dioxide (CO2) is the same in all seven models and the reservoir pressure is relatively lower in the homogeneous rock volume, accumulating the entire CO2 volume below a single sealing layer, as is the case with model 7, may increase the risk of sealing failure, which may lead to seismicity or leakage. As a result, distributing the volume of injected CO2 over multiple reservoirs that each have their own seal would be a much safer and preferable site to permanently store CO2 even if these heterogeneous rock volumes have lower pore volumes.

Through a comparative analysis of the cumulative mass of carbon dioxide (CO2) injected into reservoirs over 50 years across all seven models, the models are ranked in terms of their efficiencies in storing CO2 over time, as shown below:

Ranking of the Models	Efficiency
Model 1 & Model 4	Best
Model 2	
Model 5 & Model 6	lower ↓ ↑ higher
Model 3	
Model 7	Worst

7.2. Advantages and Limitations of the Modelling Approaches

The methodology used in constructing all seven geo-models exhibits a high level of efficiency in conducting screening assessments related to the influence of reservoir heterogeneity on the development of CO2 plumes. The utilization of a sketch-based modeling approach in Rapid Reservoir Modeling (RRM) facilitates the rapid creation of three-dimensional representations of outcrops or conceptual models, enabling efficient studying of various scenarios within a limited time-frame. Nevertheless, this modeling approach has certain limitations. The constructed models are deterministic, lacking the capability to incorporate probability distributions as stochastic techniques do. In addition, the sketch-based modeling approach does not include the provision for post-submission surface editing. Furthermore, it should be noted that flow diagnostics neglect the influence of gravity forces in the governing equations, which emphasizes the need to employ DARTS in dynamic modeling, although it helped in selecting the location of the injection well due to fast response and on-the-fly results.

Delft Advanced Research Terra Simulator (DARTS) was employed as a robust simulation tool to model the injecting supercritical CO2 into the Roda Sandstone reservoir. DARTS possesses a multitude of advantages. One notable benefit is having the ability to operate in various energy applications, including geothermal, enhanced oil recovery (EOR), and subsurface storage while considering essential physical aspects such as gravity, viscosity, density, and other variables. An additional benefit lies in its capacity to efficiently handle high-resolution models, specifically those containing small-scale heterogeneities. Moreover, the ability to modify the parameters is one of the advantages associated with utilizing DARTS. Nevertheless, DARTS does have certain restrictions. A comprehensive understanding of reservoir simulation is necessary in order to comprehend the functioning of the simulator, execute the models, and rightfully validate the outcomes. Moreover, proficiency in Python is a prerequisite for setting up the project and assigning the dynamic parameters. The last limitation associated with the utilization of DARTS pertains to the requirement of using high-performance computers when executing huge high-resolution models.

7.3. Uncertainties

The investigation into the impact of reservoir heterogeneity on CO2 plume development introduces several sources of uncertainty that can influence the accuracy and reliability of the results. Within this project, two primary sections stand out as having the most significant uncertainties: the reservoir and the injection scheme.

Regarding the reservoir, six key sources of uncertainty come into play. First and foremost are the petrophysical properties, which play a crucial role in determining how CO2 plumes develop, especially in tight reservoirs. Secondly, dynamic properties present another potential factor that can considerably alter the results. The third and fourth sources of uncertainty lie in the reservoir conditions and fluid properties, such as fluid density and compressibility, which have the capacity to impact the overall outcomes.

Additionally, the presence of impurities within the reservoir can contribute to divergent findings, thus making it another noteworthy source of uncertainty. Lastly, the existence of structural and geomechanical elements within the reservoir cannot be overlooked, as they undeniably possess the potential to alter the flow path of injected CO2.

In the injection scheme, four primary aspects may introduce uncertainty. These aspects include the properties of the injected fluid, the chosen injection type (continuous or cyclic), the design of the injection wells (geometry and completion), and the injection pattern (single well or multi-wells). Each of these aspects has the capacity to cause variations in the development and migration of the CO2 plume within the reservoir.

By acknowledging and addressing these key sources of uncertainty in both the reservoir and injection scheme sections, a more comprehensive understanding of CO2 plume development in heterogeneous reservoirs can be achieved. Through careful consideration of these uncertainties, it becomes possible to make informed decisions and draw meaningful conclusions from the study.

8

Conclusion

The Ypresian Roda sandstone formation consists of multiple Gilbert-delta lobes and sub-lobes. These lobes are composed mainly of porous sandstones. Between these sand bodies, carbonate-cemented layers were developed. The degree of lithification development of these layers depends on the cessation of the sediments period and the presence of carbonate nuclei simultaneously. Different levels of lithification are possible, therefore this thesis research considers a range of outcomes.

The presence of reservoir heterogeneities, particularly the impermeable cemented layers within the Roda sand bodies, has played a significant role in shaping the evolution of the CO2 plume over five decades. In a nutshell, the dominant factor influencing the flow direction of CO2 in the homogeneous rock volume is buoyancy. This results in the immediate rising of CO2 from the injection borehole, bypassing a significant portion of the rock volume. Consequently, despite having a higher pore volume, a substantial portion of the rock volume is not utilized for storage. In contrast, the presence of laterally continuous impermeable layers within a heterogeneous rock volume, even with variations in their thicknesses, leads to the dispersion of CO2 plumes' flow path. This dispersion ultimately results in an increased percentage of the contacting area between the CO2 and the rock volume. As a result, the storage capacity of this buoyant fluid is enhanced by having more CO2 volumes in the lower parts of the rock volume as CO2 is distributed along the impermeable layers. Similarly, when the carbonate-cement layers have not fully developed and continued laterally (patchy cement scenarios), there was a significantly increased accessible volume of porosity. This can be attributed to the intricate flow pathways that the CO2 followed.

The probability of sealing failure, which might cause seismicity or leaking, is increased if the whole volume of the CO2 is accumulated beneath an individual sealing layer. Therefore, it is considerably more secure and efficient to store CO2 permanently across several reservoirs, each of which has its own seal. Several uncertainties may affect outcomes in terms of reliability and accuracy. The reservoir conditions and parameters as well as the injection strategy, can contribute to introducing a high amount of uncertainty that can alter the findings and lead to a different conclusion.

At the end of the project, I would like to recommend four points to be considered in future projects. The first is to examine the CO2 plume behaviors in different depositional environments such as fluvial, marine carbonate, glacial, etc. The second recommendation is to integrate sedimentological heterogeneity with structural and geomechanical elements in a single model in order to see the flow path of CO2 and storage efficiency in complex systems. Additionally, conducting a sensitivity analysis of the dynamic parameters and injector locations is highly recommended. The last point is to integrate the CO2 storage study with EOR technology since EOR is well-known and widely used.

References

[1] Catherine M Gibson-Poole et al. “Understanding stratigraphic heterogeneity: a methodology to maximize the efficiency of the geological storage of CO2”. In: (2009).

[2] Temitope Ajayi et al. “A review of CO2 Storage in geological formations emphasizing modeling, monitoring and capacity estimation approaches”. In: *Petroleum Science* 16.5 (July 2019), pp. 1028–1063. DOI: 10.1007/s12182-019-0340-8.

[3] Bert Metz et al. “IPCC special report on carbon dioxide capture and storage”. In: (July 2005). URL: https://www.osti.gov/biblio/20740954.

[4] Puigdefàbregas C. et al. “Tecto-sedimentary cycles and depositional sequences of the Mesozoic and tertiary from the pyrenees”. In: *Tectonophysics* 129.1–4 (Oct. 1986), pp. 173–203. DOI: 10.1016/0040-1951(86)90251-9.

[5] Dewey J.F. et al. “Kinematics of the western Mediterranean”. In: *Geological Society, London, Special Publications* 45.1 (Jan. 1989), pp. 265–283. DOI: 10.1144/gsl.sp.1989.045.01.15.

[6] Srivastava S.P. et al. “Motion of iberia since the late Jurassic: Results from detailed aeromagnetic measurements in the Newfoundland Basin”. In: *Tectonophysics* 184.3–4 (Dec. 1990), pp. 229–260. DOI: 10.1016/0040-1951(90)90442-b.

[7] Roest W.R. et al. “Kinematics of the plate boundaries between Eurasia, Iberia, and Africa in the North Atlantic from the late cretaceous to the present”. In: *Geology* 19.6 (June 1991), p. 613. DOI: 10.1130/0091-7613(1991)019<0613:kotpbb>2.3.co;2.

[8] Olivet J-L. “La cinématique de la plaque ibérique”. In: *Bulletin des centres de recherches exploration-production Elf-Aquitaine* 20.1 (1996), pp. 131–195.

[9] Garrido et al. “Síntesis geologica del Secundario y Terciario entre los rios Cinca y Segre (Pirineo central de la vertiente surpirenaica, provincias de Huesca y Lérida)”. In: *Boletín Geológico y Minero* 83 (Jan. 1972), pp. 1–47.

[10] Muñoz Josep Anton. “Evolution of a continental collision belt: ECORS-pyrenees crustal balanced cross-section”. In: *Thrust Tectonics* (1992), pp. 235–246. DOI: 10.1007/978-94-011-3066-0_21.

[11] Gibbons Wes et al. “the Alpine System North of the Betic Cordillera”. In: *The geology of Spain*. Geological Society, 2002, pp. 370–385.

[12] Meigs Andrew J. “Sequential development of selected pyrenean thrust faults”. In: *Journal of Structural Geology* 19.3–4 (Mar. 1997), pp. 481–502. DOI: 10.1016/s0191-8141(96)00096-x.

[13] Bond R.M. et al. “Inversion of a Lower Cretaceous extensional basin, South Central Pyrenees, Spain”. In: *Geological Society, London, Special Publications* 88.1 (Jan. 1995), pp. 415–431. DOI: 10.1144/gsl.sp.1995.088.01.22.

[14] McClay K.R. et al. “4-D evolution of Rift Systems: Insights from scaled physical models”. In: *AAPG Bulletin* 86 (2002). DOI: 10.1306/61eedbf2-173e-11d7-8645000102c1865d.

[15] Eichenseer H. *Facies Geology of Late Maestrichtian to Early Eocene Coastal and Shallow Marine Sediments, Tremp-Graus Basin, Northeastern Spain*. Arbeiten aus dem Institut und Museum für Geologie und Paläontologie der Universität Tübingen. Herbert Eichenseer, 1988. URL: https://books.google.com.sa/books?id=TBDJzQEACAAJ.

[16] López-Blanco M. “Estratigrafia Secuencial de Sistemas Deltaicos en Cuencas de Antepais: Ejemplos de Sant Lorenc del Mont, Montserrat y Roda (Paleogeno, Cuenca de Antepais Surpirenaica)”. In: *Ph.D. Thesis, Universitat de Barcelona, Spain* (1996).

[17] Mey P.H.W. et al. “Lithostratigraphic subdivision of Post-Hercynian deposits in the South-Central Pyrenees, Spain”. In: *Leidse Geologische Mededelingen* 41.1 (Jan. 1968), pp. 221–228.

[18] Schaub H. “La seccion de Campo (prov. de Huesca), XIII Coloquio Europeo de Micropaleontologia; Zona Pirenaica”. In: *Com Nac de Geologie, Madrid, Spain* (Apr. 1973), pp. 151–158.

[19] Nijman W. et al. *The Eocene Montañana Delta: Tremp-Graus Basin, Provinces of Lérida and Huesca, Southern Pyrenees, N. Spain)*. Vakgroep Sedimentologie, Rijksuniveriteit Leiden-Utrecht, 1975. URL: https://books.google.com.sa/books?id=qeZQywAACAAJ.

[20] Samso J.M. et al. “Los géneros Alveolina y Nummulites (Macroforanimíferos) de Ilerdiense Medio-Cuisiense medio de la Cuenca de Graus, Huesca. II: Sistemática de Nummulites”. In: *Geol. Min.* 101.02 (Apr. 1990), pp. 219–252.

[21] Molenaar N. et al. “Early diagenetic alteration of shallow-marine mixed sandstones: An example from the Lower Eocene Roda Sandstone Member, Tremp-Graus Basin, Spain”. In: *Sedimentary Geology* 55.3–4 (Mar. 1988), pp. 295–318. DOI: 10.1016/0037-0738(88)90136-4.

[22] Nio S.D. et al. “Sequence stratigraphic setting and sedimentary facies development of the Roda Sandstone Member”. In: *International Geoservices B.V, Sequence Stratigraphy of the Lower Tertiary Tremp-Graus Basin* (Mar. 1990), pp. 6–27.

[23] Nio S.D. et al. “Sea-level fluctuations and the geometric variability of tide-dominated sandbodies”. In: *Sedimentary Geology* 70.2–4 (Mar. 1991), pp. 161–193. DOI: 10.1016/0037-0738(91)90140-9.

[24] Michaud K. et al. “Facies, architecture and stratigraphic occurrence of headland-attached tidal sand ridges in the Roda Formation, Northern Spain”. In: Feb. 2016, pp. 313–341. DOI: 10.1002/9781119218395.ch17.

[25] Tosquella J. “Estudi sedimentologic i bioestratigr ‘ a‘fic de la Formacio Gresos de Roda (Eoc ´ e, Conca de Tremp- ‘ Graus)”. In: *M.Sc. thesis, Universitat de Barcelona, Barcelona, Spain* (1988), 183 p.

[26] Crumeyrolle P.H. et al. “Association des Sedimentologistes Francais Guide de l”. In: *Architecture et facies d’un prisme deltaique de bas niveau marin: Les gres de Roda*. Vol. 36. Paris, France, 1992.

[27] López-Blanco M. et al. “Low-amplitude, synsedimentary folding of a deltaic complex: Roda Sandstone (lower eocene), south-pyrenean foreland basin”. In: *Basin Research* 15.1 (Feb. 2003), pp. 73–96. DOI: 10.1046/j.1365-2117.2003.00193.x.

[28] Nio S.D. et al. “A Lower Eocene estuarine-shelf complex in the Isabena Valley”. In: *Sedimentology Group Report* 18 (1978).

[29] Puigdefabregas C. et al. “An Early Eocene tidal fan delta, Roda and San Esteban formations, southern Pyrenees (abs)”. In: *Abstract Book of the International Symposium on Fan Deltas, Sedimentology and Tectonic Settings*. Ed. by W Nemec et al. Bergen, Norway, 1987, pp. 143–144.

[30] Yang C.S. et al. “An ebb-tide delta depositional model—a comparison between the modern eastern Scheldt tidal basin (Southwest Netherlands) and the Lower Eocene Roda Sandstone in the Southern Pyrenees (Spain)”. In: *Sedimentary Geology* 64.1–3 (Aug. 1989), pp. 175–196. DOI: 10.1016/0037-0738(89)90091-2.

[31] Molenaar N. et al. “Fossiliferous intervals and sequence boundaries in shallow marine, fan-deltaic deposits (Early Eocene, southern Pyrenees, Spain)”. In: *Palaeogeography, Palaeoclimatology, Palaeoecology* 121.3 (1996), pp. 147–168. DOI: https://doi.org/10.1016/0031-0182(95)00073-9. URL: https://www.sciencedirect.com/science/article/pii/0031018295000739.

[32] Crumeyrolle P.H. “Stratal architecture and facies assemblages of the Roda Sandstone lowstand wedge (south-central Pyrenees)”. In: *AAPG International Conference and Exhibition*. Barcelona, Spain, 2003.

[33] Tinterri R. “The Lower Eocene Roda Sandstone (South-Central Pyrenees): An example of a flood-dominated river-delta system in a tectonically controlled basin”. In: *Rivista Italiana di Paleontologia e Stratigrafia* 113 (2007), pp. 223–255.

[34] Dubrule O. et al. “From sedimentology to geostatistical reservoir modeling”. In: *Modeling the Earth for Oil Exploration* (1994), pp. 19–114. DOI: 10.1016/b978-0-08-042419-4.50007-5.

[35] Orton G.J. et al. “Variability of deltaic processes in terms of sediment supply, with particular emphasis on grain size”. In: *Sedimentology* 40.3 (June 1993), pp. 475–512. DOI: 10.1111/j.1365-3091.1993.tb01347.x.

[36] Postma G. et al. “Architecture and sedimentary facies evolution of a marine, expanding outer-arc half-graben (crete, late Miocene)”. In: *Basin Research* 5.2 (June 1993), pp. 103–124. DOI: 10.1111/j.1365-2117.1993.tb00060.x.

[37] Dalrymple R.W. “Facies Models: Response to Sea Level Change, Geological Association of Canada”. In: (1992). Ed. by R G Walker et al., pp. 195–218.

[38] Robert Dalrymple. “Tidal depositional systems”. In: Jan. 2010, pp. 201–231.

[39] Coll M. et al. “Architectural characterization of a delta-front reservoir analogue combining Ground Penetrating Radar and Electrical Resistivity Tomography: Roda Sandstone (Lower Eocene, Graus-Tremp basin, Spain)”. In: *Geologica Acta* 11 (Mar. 2013), p. 27. DOI: 10.1344/105.000001778.

[40] Martinius A. W. et al. “A Coral-Mollusc (Goniaraea-Crassatella) Dominated Hardground Community in a Siliciclastic-Carbonate Sandstone (The Lower Eocene Roda Formation, Southern Pyrenees, Spain)”. In: *PALAIOS* 6.2 (1991), pp. 142–155. URL: http://www.jstor.org/stable/3514879 (visited on 07/11/2023).

[41] Molenaar N. et al. “Origin of nodules in mixed siliciclastic-carbonate sandstones, the Lower Eocene Roda Sandstone Member, Southern Pyrenees, Spain”. In: *Sedimentary Geology* 66.3–4 (Mar. 1990), pp. 277–293. DOI: 10.1016/0037-0738(90)90064-z.

[42] Leren Beate L.S. et al. “Controls on stratigraphic architecture in contemporaneous Delta Systems from the Eocene Roda Sandstone, tremp-graus basin, Northern Spain”. In: *Sedimentary Geology* 229.1–2 (July 2010), pp. 9–40. DOI: 10.1016/j.sedgeo.2010.03.013.

[43] NPD NPD FactPages. *31/2-1*. 2023. URL: https://factpages.npd.no/en/wellbore/pageview/exploration/all/398.

[44] Clarehugh L. “Carbonate cemented horizons within the marls of the Esdolomada Member, Roda Formation, Northern Spain: a commonly used reservoir analogue”. PhD thesis. 2018.

[45] Martinius A. W. “Multiscale gilbert-type delta lobe architecture and heterogeneities: The case of the roda sandstone member”. In: *AAPG Bulletin* 101.04 (Apr. 2017), pp. 453–463. DOI: 10.1306/011817dig17024.

[46] Mario Costa Sousa et al. “Smart Modelling of Geologic Stratigraphy Concepts using Sketches”. In: *Smart Tools and Apps for Graphics - Eurographics Italian Chapter Conference*. Ed. by Silvia Biasotti et al. The Eurographics Association, 2020. DOI: 10.2312/stag.20201243.

[47] Carl Jacquemyn et al. “Sketch-based interface and modelling of stratigraphy and structure in three dimensions”. English. In: *Journal of the Geological Society* 178.4 (July 2021). DOI: 10.1144/jgs2020-187.

[48] Carl Jacquemyn et al. *Rapid Reservoir Modelling*. 2022.

[49] William A. Jackson et al. “A screening assessment of the impact of sedimentological heterogeneity on CO2 Migration and stratigraphic-baffling potential: Johansen and Cook Formations, northern lights project, offshore norway”. In: *International Journal of Greenhouse Gas Control* 120 (2022), p. 103762. DOI: 10.1016/j.ijggc.2022.103762.

[50] Jafar Alshakri et al. “A screening assessment of the impact of sedimentological heterogeneity on CO₂ migration and stratigraphic-baffling potential: Sherwood and Bunter sandstones, UK”. In: *Geological Society, London, Special Publications* 528.1 (2023), SP528-2022–34. DOI: 10.1144/SP528-2022-34. eprint: https://www.lyellcollection.org/doi/pdf/10.1144/SP528-2022-34. URL: https://www.lyellcollection.org/doi/abs/10.1144/SP528-2022-34.

[51] Christine Doughty et al. “Capacity investigation of brine-bearing sands of the Frio Formation for geologic sequestration of CO2”. In: (Jan. 2001).

[52] Emad A. Al-Khdheeawi et al. “Impact of reservoir wettability and heterogeneity on CO2-plume migration and trapping capacity”. In: *International Journal of Greenhouse Gas Control* 58 (2017), pp. 142–158. DOI: https://doi.org/10.1016/j.ijggc.2017.01.012. URL: https://www.sciencedirect.com/science/article/pii/S1750583616305072.

[53] Roland Span et al. “A New Equation of State for Carbon Dioxide Covering the Fluid Region from the Triple□Point Temperature to 1100 K at Pressures up to 800 MPa”. In: *Journal of Physical and Chemical Reference Data* 25.6 (Nov. 1996), pp. 1509–1596. DOI: 10.1063/1.555991. eprint: https://pubs.aip.org/aip/jpr/article-pdf/25/6/1509/11996481/1509_1_online.pdf. URL: https://doi.org/10.1063/1.555991.

[54] Nozomu Yoshida et al. “Investigation of uncertainty in CO2 Reservoir Models: A sensitivity analysis of relative permeability parameter values”. In: *International Journal of Greenhouse Gas Control* 49 (June 2016), pp. 161–178. DOI: 10.1016/j.ijggc.2016.03.008.